



ORIGINAL ARTICLE

Improved corrosion resistance of mild steel in acidic solution by hydrazone derivatives: An experimental and computational study

Hassane Lgaz^a, Ill-Min Chung^{a,*}, Mustafa R. Albayati^b, Abdelkarim Chaouiki^c, Rachid Salghi^c, Shaaban K. Mohamed^{d,e}

^a Department of Crop Science, College of Sanghur Life Science, Konkuk University, Seoul 05029, South Korea

^b Department of Chemistry, College of Education, Kirkuk University, Kirkuk, Iraq

^c Laboratory of Applied Chemistry and Environment, ENSA, University Ibn Zohr, PO Box 1136, Agadir, Morocco

^d Faculty of Science and Engineering, Health Care Division, Manchester Metropolitan University, Manchester M1 5GD, England, United Kingdom

^e Chemistry Department, Faculty of Science, Minia University, 61519 El-Minia, Egypt

Received 26 April 2018; accepted 5 August 2018

Available online 16 August 2018

KEYWORDS

Mild steel;
Corrosion inhibition;
HCl;
Hydrazone derivative;
Modelling studies

Abstract Poor corrosion resistance of mild steel (MS) is a serious concern in many industrial applications. Application of corrosion inhibitors is a possible solution to combat steel corrosion. As yet, there is very little research reported focusing on hydrazone derivatives as corrosion inhibitors, here we present a combined experimental and theoretical study of the adsorption of three newly synthesized hydrazones (HDZs), namely, (E)-N'-(4-(dimethylamino)benzylidene)-2-((2,3-dimethylphenyl)amino)benzohydrazide (HDZ-1), (E)-2-((2,3-dimethylphenyl)amino)-N'-(4-methylbenzylidene)benzohydrazide, (HDZ-2) and (E)-N'-(benzylidene)-2-((2,3-dimethylphenyl)amino)benzohydrazide (HDZ-3) on the MS surface in 1 M HCl. The interaction of HDZs and the metal surface was investigated using electrochemical techniques, X-ray photoelectron spectroscopy (XPS), DFT and molecular dynamic (MD) simulations. XPS shows that inhibitor molecules form a stable layer on steel surface through chemical and physical interactions. HDZs adsorption onto the steel surface was found to follow Langmuir model. Furthermore, electrochemical measurement results demonstrated that our developed inhibitors act as of mixed-type (anodic and cathodic), with HDZ-1 showing the highest polarization resistance and lowest corrosion current density. Scanning electron microscope (SEM) was used to examine the surface morphology of the steel samples. The new

* Corresponding author.

E-mail address: imcim@konkuk.ac.kr (I.-M. Chung).

Peer review under responsibility of King Saud University.



Production and hosting by Elsevier

<https://doi.org/10.1016/j.arabjc.2018.08.004>

1878-5352 © 2018 Production and hosting by Elsevier B.V. on behalf of King Saud University.

This is an open access article under the CC BY-NC-ND license (<http://creativecommons.org/licenses/by-nc-nd/4.0/>).

hydrazones showed significantly improved steel corrosion resistance, which provides opportunities to explore the inhibitive activity of structurally similar compounds.

© 2018 Production and hosting by Elsevier B.V. on behalf of King Saud University. This is an open access article under the CC BY-NC-ND license (<http://creativecommons.org/licenses/by-nc-nd/4.0/>).

1. Introduction

Mild steel has been used extensively in the oil, gas and chemical industries because of its outstanding mechanical properties. The use of steel is also one of the effective strategies to maximize profit and reduce cost as compared to expensive corrosion resistant alloys (Abdel-Rehim et al., 2011; Laamari et al., 2016; Umoren et al., 2016). However, this alloy still suffers from corrosion when it comes in contact with corrosive environments, especially those containing chloride ions (Dwivedi et al., 2017). In many industrial applications related to oil and gas processing such as pipeline cleaning, pipeline/acid descaling and oil well acidizing, the use of mineral acids (usually hydrochloric acid) is still an effective method for improving productivity (Lgaz et al., 2017a). Effective ways to prevent corrosion of metals adopted by some industries include materials selection, and cathodic protection amongst others. However, these methods are very expensive, which is unreasonable in practical applications. As far as acidic media is concerned, the use of organic inhibitors is one of the practical methods to combat the menace of corrosion due to its advantages of economy and high efficiency (Abdul Rahiman and Sethumanickam, 2017; Chidiebere et al., 2014). Organic compounds containing heteroatoms (in particular N, O, S, and P) could act as an effective barrier and provide strong protection by adsorbing onto the metallic surfaces and blocking one or more of the corrosion reactions occurring at the solution/metal interface (Esmaeili et al., 2015). The adsorbability of an organic compound is strongly dependent on the planar form, aromatic rings, the nature of functional groups, steric as well as electronic factors (Yilmaz et al., 2016). Considering the well-known toxicity of efficient inorganic inhibitors and the concern about environmental hazards, great efforts have been made to develop alternative substances that are effective enough and environmentally friendly. A great deal of research has focused on investigating inhibitive properties of a large variety of biocompatible green corrosion inhibitors in an effort to describe, and understand their inhibition mechanism (Umoren et al., 2016). Recently, Mehdipour et al. reported the effects of Aloe plant extract on stainless steel corrosion in 1 M H₂SO₄ using electrochemical and surface characterization techniques (Mehdipour et al., 2015). They found that Aloe plant extract acted as a good corrosion inhibitor for the stainless steel in sulfuric acid solution and its adsorption on the metal surface followed the Langmuir adsorption isotherm. The authors reported that the presence of many heteroatoms in the Aloe compounds was the reason for its effective protection of stainless steel. The effectiveness of an organic/inorganic hybrid green corrosion inhibitive pigment for corrosion protection of mild steel in chloride solution was studied by Salehi et al. (2017). They showed that the green hybrid organic/inorganic complex effectively protected mild steel

through deposition of a protective film on the steel surface. On the other hand, Feng et al. (2018) found excellent results for corrosion inhibition of X70 steel in acidic medium using three ionic liquids with different anionic carbon chain lengths as green inhibitors. A green eco-friendly mixture comprised of glucomannan and bis-quaternary ammonium salt has also been used as corrosion inhibitors for the protection of mild steel in simulated seawater (Luo et al., 2017). The authors found that the mixture acts as an effective inhibitor and its adsorption on mild steel surface achieved by the chemical as well as physical adsorption. These results and others (Alibakhshi et al., 2018; Sanaei et al., 2017; Verma et al., 2018) reflect the increasing general interest in this research field.

Inspired by the above successful cases, we designed and successfully prepared new potent organic inhibitors carrying mefenamic acid. Mefenamic acid (2-(2,3-dimethylphenyl)aminobenzoic acid) belongs to non-steroidal Anti-Inflammatory Drugs (NSAID's) which are classified as an important class of therapeutic agents (Aronson, 2016). It is one of the most common drugs to the treatment of mild to moderate pain along with other diseases (Antonio and Maggio, 2018; Joo et al., 2006). Functionalization of the free carboxylic group in MA like other NSAIDs could control the most effective side effect of these drugs such as gastrointestinal toxicity (Mohamed et al., 2015). One of the most effective functionalization of carboxylic group is the conversion into hydrazone derivatives (Almasirad et al., 2005). In addition to the various biological activities of hydrazones (Rollas and Küçükgülzel, 2007), a widespread applications have been reported in many research fields (Mendoza et al., 2012). However, a little work has been reported on the use of hydrazones in the field of corrosion inhibition (Fouda Abd El-Aziz et al., 2006).

The aim of this study was to develop a better understanding of mechanisms related to corrosion inhibition process of mild steel in 1 M HCl using three hydrazone derivatives, namely, (E)-N'-(4-(dimethylamino)benzylidene)-2-((2,3-dimethylphenyl)amino)benzohydrazide (HDZ-1), (E)-2-((2,3-dimethylphenyl)amino)-N'-(4-methylbenzylidene)benzohydrazide, (HDZ-2) and (E)-N'-benzylidene-2-((2,3-dimethylphenyl)amino)benzohydrazide (HDZ-3) which may provide a platform for further investigations of structurally similar compounds. To the best of our knowledge, no such research has been conducted. The inhibitive effects of hydrazone derivatives on MS corrosion in 1 M HCl were monitored through weight loss and electrochemical techniques complemented with surface morphology characterization using SEM. To shed light on the mechanism of molecular adsorption, further investigations by X-ray photoelectron spectroscopy (XPS), Density Functional Theory (DFT), Molecular dynamics simulation (MDS) and Radial distribution function (RDF) were also performed.

2. Experimental

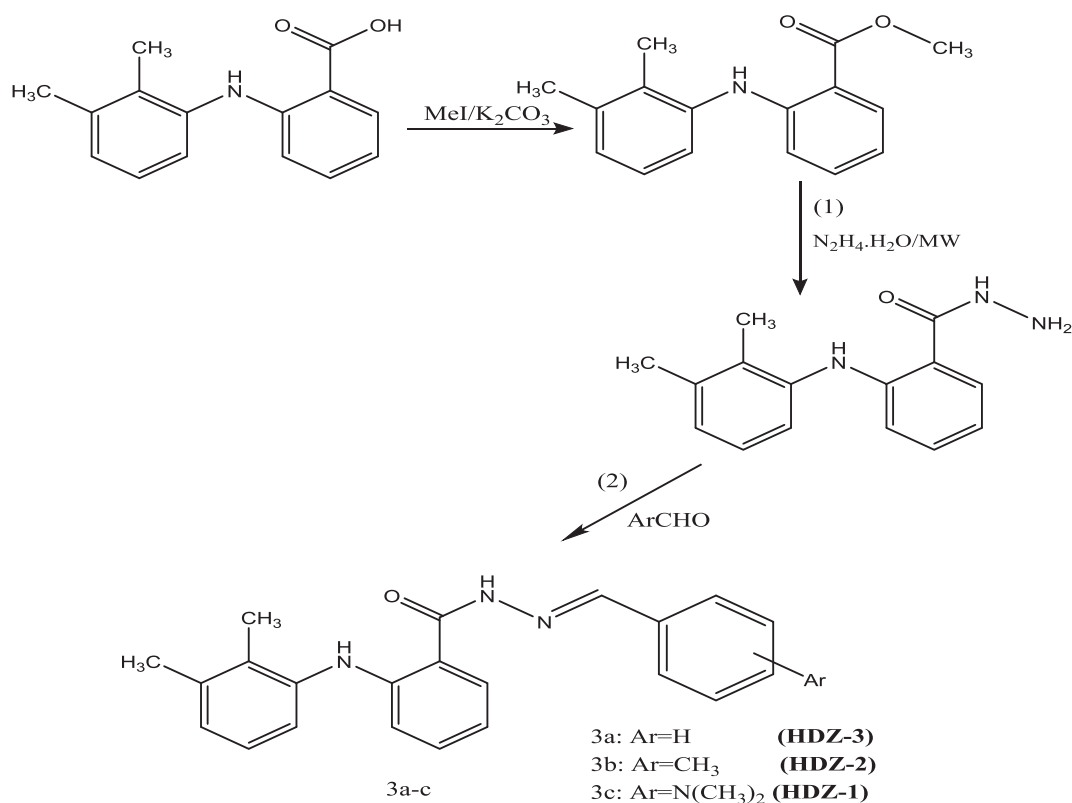
2.1. Synthesis

All chemicals were obtained from Sigma (Merck) and used as received. Melting points were recorded using Stuart melting point apparatus SMP30 (Bibby Scientific). The IR spectra were measured using FTIR spectrometer (Nicolet 380, Thermo Electron Corporation, USA). The ^1H NMR and ^{13}C NMR spectra were recorded with Bruker 400 MHz in DMSO. [Scheme 1](#) represents the general procedure for synthesis of hydrazones (3a-c) (see [Scheme 2](#)).

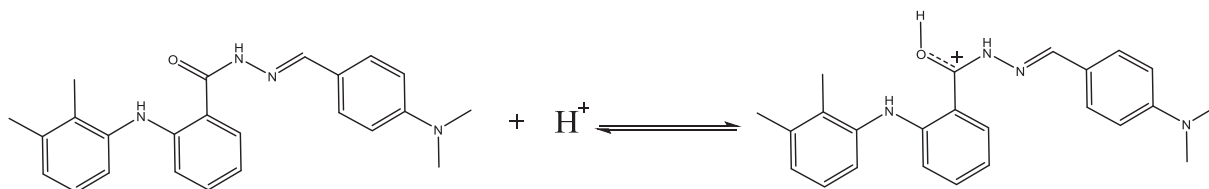
Synthesis and characterization of methyl 2-[(2,3-dimethylphenyl)amino]benzoate (1): A mixture of (2.0 mg, 8.28 mol) Mefenamic acid and (2.0 mg, 16.6 mmol) anhydrous potassium carbonate was added to dry acetone (80 ml) and stirred for 60 min. Then Excess of Methyl Iodide (3.6 mg, 24.8 mmol) was added. The resulting mixture was refluxed for 18 h. The reaction mixture was filtered when hot and the resultant cakes were

washed with dry acetone (6×2 ml). The filtrate was evaporated under reduced pressure to afford the ester as an oily material, solidified after 4 days at room temperature with m.p = 100–102 °C. IR(KBr): ($\text{C}=\text{O}$ ester 1725 cm^{-1}), (NH 3332 cm^{-1}), ($\text{C}-\text{H}$ aliphatic $2999\text{--}2943\text{ cm}^{-1}$), ($=\text{C}-\text{H}$ aromatic 3012 cm^{-1}).

Synthesis and characterization of 2-[(2,3-dimethylphenyl)amino]benzohydrazide (2): A mixture of Mefenamic acid methyl ester (1) (1 mmol) and hydrazine hydrate (85%, 2.5 mmol) was irradiated, in closed vessel, under microwave irradiation at 300 W and 2500 °C for 7 min. The reaction mixture was cooled, the separated solid was washed with water, filtered, dried and recrystallized from ethanol to afford the hydrazide (2) with m.p = 119–121 °C. IR(KBr): ($\text{C}=\text{O}$ amide 1654 cm^{-1}), (NH 3290 cm^{-1}), (NH_2 , $3290\text{--}3309\text{ cm}^{-1}$), ($\text{C}-\text{H}$ aliphatic 2949 cm^{-1}), ($=\text{C}-\text{H}$ aromatic 3018 cm^{-1}). ^1H NMR (400 MHz, DMSO): $\delta = 2.1(\text{s}, 3\text{H}, \text{CH}_3)$, $2.2(\text{s}, 3\text{H}, \text{CH}_3)$, $9.4(\text{s}, 1\text{H}, \text{NH})$, $9.8(\text{br.s}, 1\text{H}, \text{NH amide})$, $3.5(\text{br.s}, 2\text{H}, -\text{NH}_2)$, $6.7\text{--}7.9(\text{m}, 7\text{H}, \text{Ar-H})$. ^{13}C NMR $\delta = 13.5(\text{CH}_3)$, $20.2(\text{CH}_3)$,



Scheme 1 Hydrazones synthesis scheme.



Scheme 2 The protonation state of the hydrazone molecule in 1 M HCl.

113.9, 115.9, 116.9, 119.6, 125.0, 125.8, 128.2, 129.3, 131.8, 137.7, 139.3, 145.9 (Aromatic carbons), 168.4 (C=O amide).

General procedure for synthesis of hydrazones(3a-c): A mixture of equimolar ratio of Mefenamic acid hydrazide and appropriate aldehydes with catalytic amount of glacial acetic acid was refluxed for 5 h. On cooling, the precipitate was separated then collected and recrystallized from ethanol to give 3a-c.

N'-(E)-4-benzylidene]-2-(2,3-dimethylanilino)benzohydrazide (3a, C₂₃H₂₂N₂O): m.p = 193–195 °C; IR(KBr): (C=O amide 1639 cm⁻¹), (NH 3199 cm⁻¹) (NH 3338 cm⁻¹), (C–H aliphatic 2947 cm⁻¹), (C=N 1597 cm⁻¹). ¹H NMR (400 MHz, DMSO): δ = 2.1(s,3H,CH₃), 2.2(s,3H,CH₃), 9.2(s,1H, NH), 9.9(s,1H,NH amide), 6.6–7.8(m,12H,aromatic), 7.9 (s,1H, –CH=N–).

¹³C NMR δ = 18(CH₃), 24(CH₃), 116, 118, 119.4, 119.5, 121, 125, 130.3, 130.7, 133.4, 134.3, 134.5, 134.6, 137, 142, 143, 150.6, 150.9, 151 (Aromatic carbons), 173(C=O amide), 162(C=N).

N'-(E)-4-methylbenzylidene]-2-(2,3-dimethylanilino)benzohydrazide (3b, C₂₄H₂₄N₂O): m.p = 196–199 °C; IR(KBr): (C=O amide 1643 cm⁻¹), (NH 3142 cm⁻¹) (NH 3350 cm⁻¹), (C–H aliphatic 2939 cm⁻¹), (C=N 1571 cm⁻¹). ¹H NMR (400 MHz, DMSO): δ = 2.07 (2,3H, CH₃), 2.2(s, 3H, CH₃), 2.4 (s,3H, CH₃), 9.2(s,1H, NH), 9.9(s,1H, NH), 6.7–7.7(m, 11H, aromatic), 7.9(s, 1H, –CH=N–). ¹³C NMR δ = 13(CH₃), 20.08(CH₃), 20.6(CH₃), 113, 114, 116, 120, 123, 125, 127, 128, 129.1, 129.7, 131, 132, 137, 138, 146, 148 (aromatic carbons), 164(C=N), 168(C=O).

N'-(E)-4-Dimethylaminobenzylidene]-2-(2,3-dimethylanilino)benzohydrazide (3c, C₂₅H₂₇N₃O): m.p = 245–248 °C; IR (KBr): (C=O amide 1658 cm⁻¹), (NH 3277 cm⁻¹), (NH 3400 cm⁻¹), (C–H aliphatic 2933 cm⁻¹), (C=N 1606 cm⁻¹). ¹H NMR (400 MHz, DMSO): δ = 2.1(s, 3H, CH₃), 2.2(s, 3H, CH₃), 2.4(s, 6H, CH₃), 11.8 (s,1H, NH), 9.2(s,1H, NH), 8.3 (s,1H, NH), 6.7–7.7(m,11H, aromatic). ¹³C NMR δ = 13 (CH₃), 20(CH₃), 29(2CH₃), 111, 114, 117, 119, 120, 121, 122, 125, 127, 130, 131, 133, 137, 138, 142, 147 (aromatic carbon), 162 (C=N), 165 (C=O).

2.2. Materials and corrosive solutions

The metal substrates used in this research were made from commercially available mild steel with a chemical composition of: 0.370% C, 0.230% Si, 0.680% Mn, 0.016% S, 0.077% Cr, 0.011% Ti, 0.059% Ni, 0.009% Co, 0.160% Cu, and balance Fe. Prior to each individual experiment, test coupons were mechanically abraded using a belt grinding polishing machine. To obtain a polished surface, mild steel surface was grounded with emery papers of 400–1600 grades and cleaned thoroughly. The test solution (1 M HCl) was prepared by diluting 37% analytical grade HCl with double distilled water.

2.3. Weight loss measurements

According to the ASTM standard (Scully and Baboian, 1995), a disk-shaped specimens (38 mm in diameter and 3 mm in thickness with a hole of 8 mm diameter) were prepared for each weight loss tests. The mild steel samples were immersed in uninhibited and inhibited solutions for 24 h at 303 K. The MS samples were prepared as mentioned previously and

weighted using a precision balance with a sensitivity of 0.1 mg. After each test, the MS specimens were taken out and rinsed thoroughly with distilled water and acetone, dried and re-weighed accurately. The experiments were carried out in triplicates and only the average values of the weight losses were reported. The following equation (Eq. (1)) was used to determine the corrosion rate in millimeters per year (mm y⁻¹):

$$C_{RW} = \frac{K \times W}{A \times t \times \rho} \quad (1)$$

where K = 8.76 × 10⁴ was used as constant. W and t are the mass loss in gram and the time of exposure in hours, respectively. According to ASTM G1-03 standard (ASTM Committee G-1 on Corrosion of Metals, 2011), the density of mild steel is 7.86 g cm⁻³. The exposed area, A (in cm²) was calculated from Eq. (2) (Salarvand et al., 2017):

$$A = \frac{\pi}{2} (D^2 - d^2) + \pi D + \pi d \quad (2)$$

where D, d, and l are the diameter of mild steel pieces, the diameter of the hole for holding and the thickness, respectively.

2.4. Electrochemical measurements

Electrochemical impedance spectroscopy (EIS) and potentiodynamic polarization (PDP) were performed using a three-electrode setup and a Volta Lab (Tacussel- Radiometer PGZ 100) potentiostat. The three-electrode system consisted of a working electrode (mild steel) with the surface area of 1 cm² in contact with the electrolyte, Pt as an auxiliary electrode alongside a saturated calomel reference electrode. Before electrochemical measurements, the working electrode was first immersed in the test solution for 30 min in order to be in equilibrium with the environment. The electrochemical measurements were performed when the OCPs became stable (Fig. S1, Supplementary material). Measurement of the impedance spectra was obtained in the frequency range of 10 mHz to 100 kHz and peak to peak perturbations of 5 mV. The Tafel polarization measurements were recorded at a scanning range of 1 mV s⁻¹ in the range from –800 to –200 mV vs. SCE at steady open-circuit potential. The electrochemical parameters were extracted from Tafel plots at ± 50 mV around E_{corr} using Tafel extrapolation method (Tkacz et al., 2016). All electrochemical measurements were performed in triplicate in a cell containing 80 ml of the electrolyte at 303 K.

Supplementary data associated with this article can be found, in the online version, at <https://doi.org/10.1016/j.arabjc.2018.08.004>.

2.5. SEM and XPS studies

Scanning electron microscopy has been used to investigate the changes in surface of the mild steel samples, before and after addition of inhibitor in 1 M HCl. The MS samples were scanned after 6, 12 and 24 h of immersion in 1 M HCl with 5 × 10⁻³ M of HDZ-1. SEM imaging was performed by a Hitachi TM-1000 SEM at an accelerating voltage of 15 kV. The spectra of XPS were recorded by a Physical Electronic PHI 5700 spectrometer with a non-monochromatic Mg-Kα radiation (300 W, 15 kV, and 1253.6 eV). High-resolution

spectra of the elements of interest were recorded by a hemispherical multichannel detector operating in the constant pass energy mode at 25.9 eV, and step size of 0.1 eV, using a 720 μm diameter analysis area. The XPS spectra were quantified using a non-linear least squares algorithm with a Shirley background and a Gaussian–Lorentzian combination. The X-ray photoelectron spectra obtained were analyzed using PHI SmartSoft software and processed using MultiPak 9.3 package.

2.6. Computational details

2.6.1. Quantum chemical calculations

All Density Functional Theory (DFT) calculations were performed on the hydrazone derivatives using Gaussian 09 package program (Frisch et al., n.d.). The visualization of results was carried out using GaussView program. Quantum chemical parameters such as the energy values of the highest occupied molecular orbital (E_{HOMO}) and the lowest unoccupied molecular orbital (E_{LUMO}), ΔE (energy gap), and fraction of electrons transferred from the inhibitors to iron surface (ΔN), were calculated using B3LYP exchange-correlation functional (Becke, 1988; Lee et al., 1988) with 6-311++G(d, p) basis set for all atoms. All DFT calculations have been done in aqueous phase (water) using polarized continuum model (PCM) (Wong et al., 1991). The Koopmans's theorem establishes a relationship between the energy of the HOMO and the ionization potential i.e. the energy required to detach an electron from an atom, a molecule, or an ion, and between the energy of the LUMO and the electron affinity, i.e. the energy released when an electron is added to a neutral atom (Gholami et al., 2013). Based on this, the electron affinity, ionization potential, electronegativity, and hardness were calculated by applying Eqs. (3)–(6) (Pearson, 1988; Sastri and Perumareddi, 1997):

The electron affinity (EA)

$$EA = -E_{\text{LUMO}} \quad (3)$$

The ionization potential (IP)

$$IP = -E_{\text{HOMO}} \quad (4)$$

Absolute electronegativity (χ)

$$\chi = \frac{IP + EA}{2} \quad (5)$$

Absolute hardness (η)

$$\eta = \frac{IP - EA}{2} \quad (6)$$

The inhibitor's tendency to electron density transfer to a metal surface can be estimated by the number of transferred electrons (ΔN) using the Eq. (7) (Martinez, 2003):

$$\Delta N = \frac{\phi - \chi_{\text{inh}}}{2(\eta_{\text{Fe}} + \eta_{\text{inh}})} \quad (7)$$

The theoretical values of the work function (ϕ) and η_{Fe} are 4.82 and 0 respectively (Cao et al., 2014; Kokalj, 2012).

2.6.2. Local reactivity analysis (Fukui indices)

The Fukui functions have been used as a useful tool to compare the local reactivity properties (Olasunkanmi et al., 2016). The condensed Fukui functions of the molecules were analyzed using the Dmol³ module implemented in Material Studio (MS) Ver. 6 (Materials Studio, 2013). B3LYP

exchange-correlation function and the double numeric with polarization (DNP) basis set have been used for all calculations. Herein, the finite difference approximation using Mulliken Population Analysis (MPA) has been used to compute the Fukui functions. The Fukui functions were proposed as follows (Mi et al., 2015):

$$f_k^+ = q_k(N + 1) - q_k(N) \quad (8)$$

$$f_k^- = q_k(N) - q_k(N - 1) \quad (9)$$

In the above equations, $q_k(N)$, $q_k(N + 1)$ and $q_k(N - 1)$ are the atomic charges of the systems with N , $N + 1$, and $N - 1$ electrons, respectively.

2.6.3. Molecular dynamic (MD) simulations

The MD simulations were carried out using Materials Studio software. This method is particularly useful in studying the interaction energies between the inhibitor molecules and the Fe (1 1 0) surface. In this simulation process, the iron crystal was imported and cleaved along (1 1 0) plane and a slab of 6 \AA was employed. The Fe (1 1 0) surface was relaxed and then, enlarged to a (10 \times 10) supercell to provide a large surface for the interaction of the inhibitor. A vacuum slab with zero thickness was built. In order to make the MD simulation closer to the real system, a supercell with a size of $24.82 \times 24.82 \times 25.14 \text{\AA}^3$ contains 491 H_2O , $9\text{H}_3\text{O}^+$, 9Cl^- and 1 inhibitor molecule was created (Salarvand et al., 2017). The simulations were performed in a simulation box ($24.82 \times 24.82 \times 35.69 \text{\AA}^3$) via Discover module implemented in MS software with COMPASS force field (Sun, 1998), a time step of 1 fs, simulation time of 2000 ps and NVT ensemble at 303 K. Information about the interactions between the corrosion inhibitors and Fe (1 1 0) surface was determined by the calculation of the interaction and binding energies using Eqs. (10) and (11) (Saha et al., 2016):

$$E_{\text{interaction}} = E_{\text{total}} - (E_{\text{surface + solution}} + E_{\text{inhibitor}}) \quad (10)$$

$$E_{\text{binding}} = -E_{\text{interaction}} \quad (11)$$

where the total energy of the entire system is defined as E_{total} , $E_{\text{surface + solution}}$ referred to the total energy of Fe (1 1 0) surface and solution without the inhibitor and $E_{\text{inhibitor}}$ represents the total energy of inhibitor.

As part of our ongoing efforts dedicated to the use of computational tools to analyze the corrosion inhibition process, we here implement the calculation of the radial distribution function from MD trajectory data. This approach has proven to be useful in a wide range of applications, including corrosion inhibition research. More details about the method and mathematical formula are available in the literature (Lgaz et al., 2017a).

3. Results and discussion

3.1. Weight loss measurements

Gravimetric tests based on mass loss measurements are still a reliable method for assessing corrosion of metals. Weight loss tests were undertaken for MS in 1 M HCl devoid of and in the presence of different concentrations of HDZ-1, HDZ-2, and HDZ-3 at 303 K. The expressions below were used to calculate

the percentage inhibition efficiency, $\eta_{WL}(\%)$ and the surface coverage (θ) (Lgaz et al., 2017a):

$$\eta_{WL}(\%) = \left[\frac{C_{RW}^{\circ} - C_{RW}}{C_{RW}^{\circ}} \right] \times 100 \quad (12)$$

$$\theta = \left[\frac{C_{RW}^{\circ} - C_{RW}}{C_{RW}^{\circ}} \right] \quad (13)$$

where C_{RW}° and C_{RW} represent the corrosion rates of the metal coupons in 1.0 M HCl before and after addition of inhibitors, respectively. Table 1 shows the gravimetric test results obtained from these experiments.

From the data in this Table, it is apparent that the corrosion rate of the samples immersed in the solutions devoid of inhibitors is significantly high (130.4 mm y^{-1}) compared to the inhibited solutions. Moreover, it is clear from the data that the corrosion rate mitigated considerably with an increase in the concentration of hydrazone derivatives. The maximal inhibition efficiency was obtained with $5 \times 10^{-3} \text{ M}$ and no further increase was observed with higher concentration of the compounds. Meanwhile, the inhibition efficiency in presence of inhibitors was found to increase continuously with an increase in the concentration of inhibitors. This is a clear indication that by increasing inhibitor concentration, there will be more and more hydrazone molecules to be adsorbed on the mild steel surface and therefore the inhibition of all corrosion forms prevailing at the metal-electrolyte interface. The order of the inhibition efficiencies at the same concentration is HDZ-1 > HDZ-2 > HDZ-3. This difference can be interpreted in terms of an electron donating powers of the three investigated hydrazones. The dimethylamino is an important donor group with Hammett substituent constant (σ) equal to -0.83 which is more negative than those of methyl group (-0.170) and H (0.00). A strong electron donating power mainly favors the

adsorption of corrosion inhibitor on the metallic surface (Singh et al., 2018). These findings are discussed in the following sections in detail.

Table 1 Corrosion rate and inhibition efficiency obtained from gravimetric measurements for mild steel samples in 1 M HCl with and without various concentration of HDZs at 303 K.

Inhibitors	Concentration/M	$C_{RW}/\text{mm y}^{-1}$	$\eta_{WL}/\%$
HCl	1.0	130.4 ± 0.6	–
	1×10^{-2}	11.7 ± 0.6	91
	5×10^{-3}	10.3 ± 0.4	92
HDZ-1	1×10^{-3}	21.2 ± 0.3	83
	5×10^{-4}	28.1 ± 0.6	78
	1×10^{-4}	32.7 ± 0.2	74
	1×10^{-2}	16.8 ± 0.3	87
	5×10^{-3}	13.5 ± 0.7	89
HDZ-2	1×10^{-3}	24.1 ± 0.6	81
	5×10^{-4}	33.2 ± 0.4	74
	1×10^{-4}	37.0 ± 0.3	71
	1×10^{-2}	20.1 ± 0.7	84
	5×10^{-3}	17.8 ± 0.2	86
HDZ-3	1×10^{-3}	26.2 ± 0.8	79
	5×10^{-4}	38.7 ± 0.3	70
	1×10^{-4}	46.0 ± 0.6	64

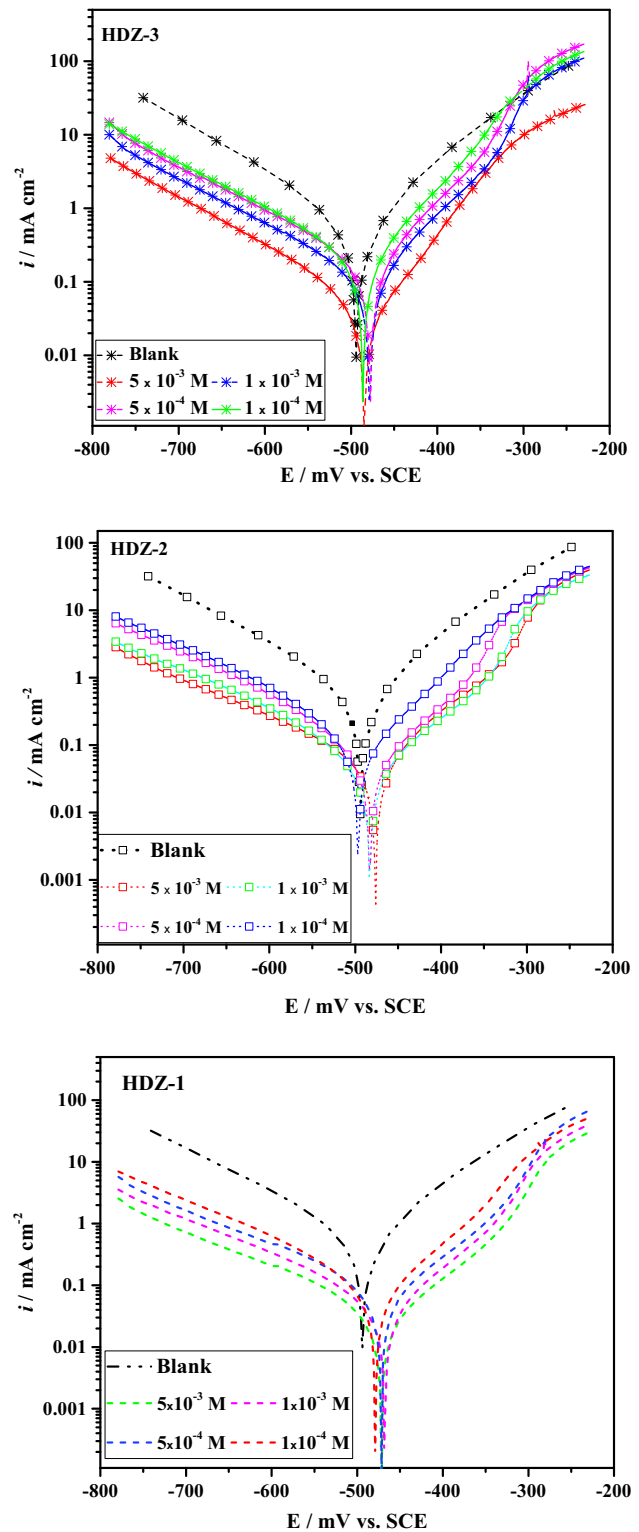


Fig. 1 Potentiodynamic polarization curves for mild steel in 1 M HCl without and with various concentrations of hydrazone derivatives at 303 K.

3.2. Potentiodynamic polarization curves

Potentiodynamic polarization technique was used to obtain information about the kinetics of the mild steel corrosion in 1 M HCl solution at different concentrations of hydrazone derivatives (Chaitra et al., 2016). Fig. 1 depicts the current–potential relationships (cathodic and anodic) for mild steel in 1 M HCl devoid of and in presence of a range of inhibitor concentrations.

Table 2 lists the polarization parameters for the uninhibited and inhibited solutions and the corresponding inhibition efficiency values which were calculated using the below expression (Lgaz et al., 2017a):

$$\eta_{\text{PDP}}(\%) = \left[1 - \frac{i_{\text{corr}}}{i_{\text{corr}}^{\circ}} \right] \times 100 \quad (14)$$

where i_{corr} and i_{corr}° represent the corrosion current densities recorded under the uninhibited and inhibited conditions, respectively.

Observation of Fig. 1 reveals that both the cathodic and anodic reactions inhibited significantly as evidenced in the shifting of the corrosion rate to lower values. Upon inspection of Fig. 1, it can be seen that when the potential goes towards positive values ~ -300 mV, the anodic branch is slightly changed. This phenomenon is well known as 'desorption potential' and may be explained as follows (El Mehdi et al., 2003): Under sufficiently positive potential conditions, the inhibitor molecules adsorbed on the steel surface commence to move away and no longer can sufficiently protect the mild steel at a higher potential than desorption potential. These results seem to be consistent with other research which found that an increase in anodic currents is mainly associated with desorption potential that alters significantly the inhibitor film (Bentiss et al., 2006). When we observed the influence of inhibitor molecules on the cathodic Tafel curves, we found that the corrosion rate decreased markedly to lower values in comparison to the blank

and all curves give rise to parallel lines which indicates that the inhibitor molecules does not modify the hydrogen evolution mechanism and the transfer reaction controls the hydrogen ion reduction (HIR).

Looking at Table 2, it is apparent that the i_{corr} values were found to decrease continuously with increase in the concentration of hydrazone derivatives following the order of $i_{\text{corr}}(\text{HDZ-3}) > i_{\text{corr}}(\text{HDZ-2}) > i_{\text{corr}}(\text{HDZ-1})$. At the same time, there are no significant changes in corrosion potential values except a slight positive shift in the case of HDZ-3. Overall, these results could be explained by assigning hydrazone derivatives as a mixed type inhibitors (Hegazy et al., 2013).

The values of the inhibition efficiency are shown in Table 2. It is also evident that the inhibition efficiency increases with increasing concentrations of hydrazone derivatives. This is because the increase in the concentration of inhibitors leads to an increase in the surface blocking of surface active sites by inhibitors. Potentiodynamic results were in perfect conformity with the results obtained from weight loss study.

3.3. Electrochemical impedance spectroscopy

Electrochemical impedance spectroscopy measurements were conducted on mild steel in 1 M HCl to clarify the kinetics of the electrode processes. Fig. 2. and S2 (supplementary material) depict EIS results in the Nyquist, Bode phase angle and Bode modulus formats. The EIS data recorded at the open-circuit potential illustrate a capacitive loop in form of depressed semicircles, which is seen in Bode plots only one time-constant. That is to say that the charge transfer process mainly controls the dissolution of mild steel in 1 M HCl solution (Lgaz et al., 2017b). By increasing concentration, a non-conducting protective layer on the mild steel surface was formed due to the adsorption of more inhibitor molecules on the metal surface replacing effectively the pre-adsorbed water molecules.

Table 2 Electrochemical parameters of potentiodynamic polarization and inhibition efficiency for mild steel samples in 1 M HCl with and without various concentration of HDZs at 303 K.

Inhibitors	Concentration/M	$-E_{\text{corr}}^{\text{a}}/\text{mV SCE}^{-1}$	$-\beta_{\text{c}}^{\text{b}}/\text{mV dec}^{-1}$	$\beta_{\text{a}}^{\text{c}}/\text{mV dec}^{-1}$	$i_{\text{corr}}^{\text{d}}/\mu\text{A cm}^{-2}$	$\eta_{\text{PDP}}/\%$
HCl	1.0	495 ± 0.7	162 ± 4.7	132 ± 3.2	566 ± 1.9	–
HDZ-1	5 × 10 ⁻³	474 ± 1.4	188 ± 3.8	49 ± 5.1	43 ± 3.8	92
	1 × 10 ⁻³	470 ± 0.7	182 ± 3.9	48 ± 4.7	63 ± 2.1	88
	5 × 10 ⁻⁴	474 ± 1.6	188 ± 6.1	55 ± 6.1	97 ± 4.3	82
	1 × 10 ⁻⁴	481 ± 1.5	179 ± 4.6	65 ± 2.3	139 ± 2.9	75
	5 × 10 ⁻³	478 ± 0.4	180 ± 5.2	59 ± 2.8	56 ± 1.8	89
HDZ-2	1 × 10 ⁻³	485 ± 4.3	183 ± 3.4	66 ± 3.6	86 ± 3.7	84
	5 × 10 ⁻⁴	485 ± 3.2	164 ± 3.9	71 ± 5.4	116 ± 2.5	79
	1 × 10 ⁻⁴	498 ± 1.3	164 ± 6.5	47 ± 2.7	174 ± 4.3	69
	5 × 10 ⁻³	485 ± 5.1	154 ± 5.4	78 ± 6.1	93 ± 1.7	83
HDZ-3	1 × 10 ⁻³	481 ± 6.1	168 ± 3.7	62 ± 3.2	121 ± 3.3	78
	5 × 10 ⁻⁴	480 ± 0.9	163 ± 5.3	74 ± 5.4	168 ± 4.3	70
	1 × 10 ⁻⁴	488 ± 1.6	167 ± 7.1	58 ± 2.9	220 ± 5.7	60

^a The standard deviation range for E_{corr} : [3.1–5.2%].

^b The standard deviation range for β_{c} : [4.3–6.4%].

^c The standard deviation range for β_{a} : [3.8–7.1%].

^d The standard deviation range for i_{corr} : [4.5–7.1%].

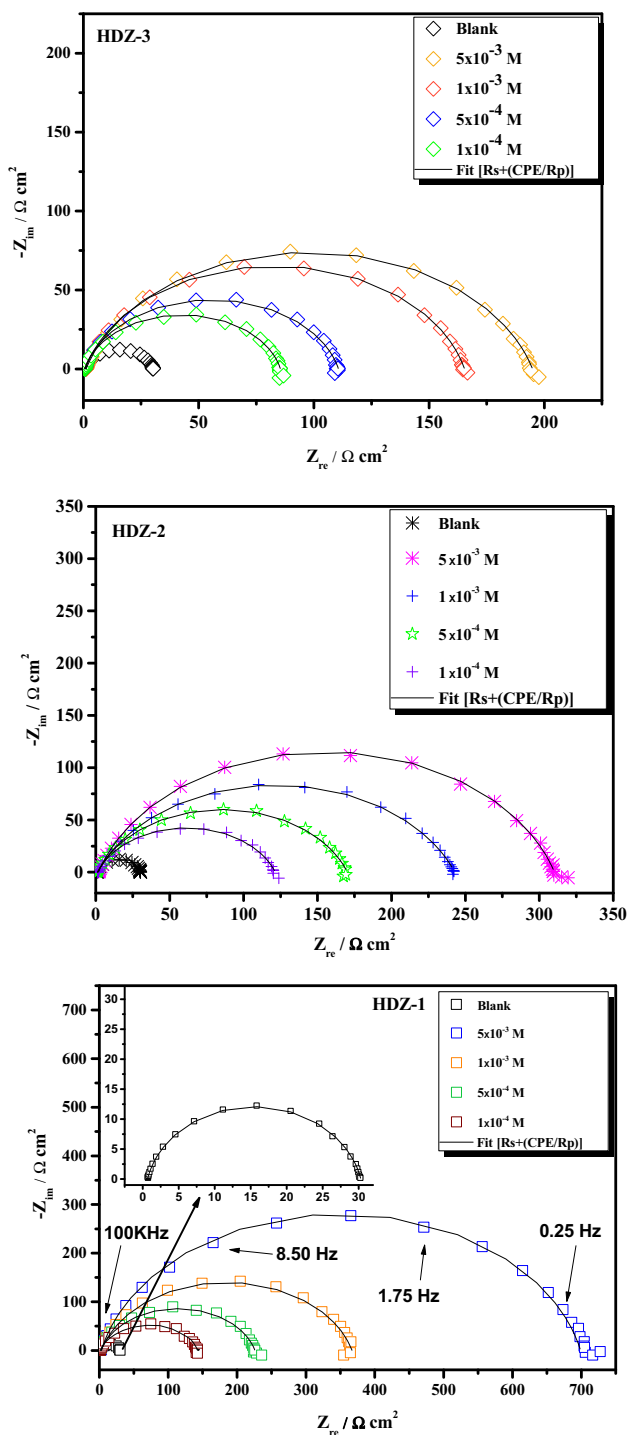


Fig. 2 EIS curves of mild steel substrate immersed in 1 M HCl solution without and with different concentrations of hydrazone derivatives at 303 K.

The EIS results of the mild steel in presence and absence of hydrazone derivatives were analyzed by fitting the experimental data to electrical equivalent circuit models using Zview software. In the proposed electrical equivalent circuit (Fig. S3, Supplementary material), R_s , represents the uncompensated solution resistance, CPE, represents the constant phase element and R_p , represents the polarization resistance which is

the sum of different resistances operating at the mild steel/electrolyte interface (El Azhar et al., 2001). The CPE is defined by the expression (Lgaz et al., 2017b):

$$Z_{CPE} = \frac{1}{Y_0(j\omega)^n} \quad (15)$$

where Y_0 is the CPE constant, ω is the angular frequency for which imaginary part of the impedance reaches its maximum (Eq. (16)) (Salarvand et al., 2017), j is the imaginary number and n is the exponential term of a CPE which gives details about the degree of surface inhomogeneity (Saha et al., 2016).

$$\omega = \left(\frac{1}{R_p Y_0} \right)^{1/n} \quad (16)$$

The interfacial capacitance C_p (sum of different capacitances operating at the mild steel/electrolyte interface) can be calculated as follows (Olasunkanmi et al., 2016):

$$C_p = \sqrt[n]{Q \times R_p^{1-n}} \quad (17)$$

The electrochemical impedance parameters such as R_s , C_p , R_p , CPE, and n as well as the $\eta_{EIS}(\%)$ values are listed in Table 3. The values of the inhibition efficiency were calculated by the following equation (Gholami et al., 2013):

$$\eta_{EIS}(\%) = \left[\frac{R_{p(inh)} - R_p}{R_{p(inh)}} \right] \times 100 \quad (18)$$

where R_p and $R_{p(inh)}$ represent the polarization resistances of the metal coupons in 1 M HCl before and after the addition of the inhibitors, respectively.

As shown in Table 3, a significant increase in polarization resistance values was observed with accompanying decrease in C_p values. The increase in R_p values implied that a protective layer was formed on the mild steel surface, thereby retarding the charge transfer process (Saha et al., 2016). Adsorbed inhibitor molecules at the mild steel/electrolyte interface replace the surface adsorbed water molecules which increase the thickness of the double layer, thus leading to the reduction of C_p values and therefore efficiently minimized dissolution of steel (Ongun Yüce et al., 2014). Like potentiodynamic polarization and weight loss results, the inhibition performances of tested compounds follow the order of HDZ-1 > HDZ-2 > HDZ-3. As expected, the presence of a strong electron-donating group (like dimethylamino group) substantially increases the reactivity of HDZ-1 and, hence, results in high inhibition efficiency.

To investigate the effect of immersion time on the inhibitor performance, EIS test was carried out in the absence and presence of 5×10^{-3} M of HDZ-1 after 6, 12, and 24 h immersion times at 303 K (Fig. 3). The electrochemical parameters at different immersion times are listed in Table 4. The results revealed that the inhibitor showed excellent performance at all immersion times. The increase in immersion time had a positive effect on inhibition efficiency which reaches its maximum at 12 h while a small decrease of 1% was observed at 24 h compared to the initial immersion time of 0.5 h. These results indicate that the tested hydrazone is an effective corrosion inhibitor and this obvious effectiveness is mainly due to the stability of the inhibitor film on the steel surface.

All in all, the comparison of the electrochemical results with weight loss data for tested compounds showed that there is a

Table 3 Electrochemical parameters of impedance and inhibition efficiency for mild steel samples in 1 M HCl with and without various concentration of HDZs at 303 K.

Inhibitors	Concentration/M	$R_p^a/\Omega\text{cm}^2$	n^b	$Q^c \times 10^{-4}/\text{Sn } \Omega^{-1} \text{cm}^{-2}$	$\chi^2 \times 10^{-3}$	$C_p/\mu\text{F cm}^{-2}$	$\eta_{\text{EIS}}/\%$
HCl	1.0	29.35 ± 1.3	0.89 ± 0.003	1.7610 ± 0.0034	0.54	91.86	–
HDZ-1	5×10^{-3}	704 ± 1.3	0.84 ± 0.003	0.2751 ± 0.0054	2.53	12	95
	1×10^{-3}	365 ± 1.1	0.83 ± 0.005	0.4994 ± 0.0012	0.89	21	91
	5×10^{-4}	224 ± 0.3	0.81 ± 0.006	0.6737 ± 0.0034	4.71	25	86
	1×10^{-4}	141 ± 1.4	0.80 ± 0.003	1.0132 ± 0.0017	3.09	35	79
HDZ-2	5×10^{-3}	307 ± 0.5	0.81 ± 0.007	0.4562 ± 0.0044	1.61	16	90
	1×10^{-3}	241 ± 0.7	0.79 ± 0.003	0.7480 ± 0.0031	0.67	25	87
	5×10^{-4}	168 ± 1.2	0.78 ± 0.004	1.1214 ± 0.0019	4.26	36	82
	1×10^{-4}	119 ± 0.9	0.80 ± 0.005	1.2596 ± 0.0027	8.04	44	75
HDZ-3	5×10^{-3}	193 ± 2.4	0.82 ± 0.004	0.8691 ± 0.0041	3.70	35	84
	1×10^{-3}	164 ± 1.3	0.85 ± 0.007	0.9932 ± 0.0033	1.03	48	82
	5×10^{-4}	110 ± 0.6	0.81 ± 0.002	1.4348 ± 0.0023	3.06	54	73
	1×10^{-4}	84 ± 1.9	0.86 ± 0.003	1.3290 ± 0.0016	8.94	64	65

^a The standard deviation range for R_p : [2.1–5.3%].

^b The standard deviation range for n : [0.3–2.9%].

^c The standard deviation range for Q : [1.2–6.8%].

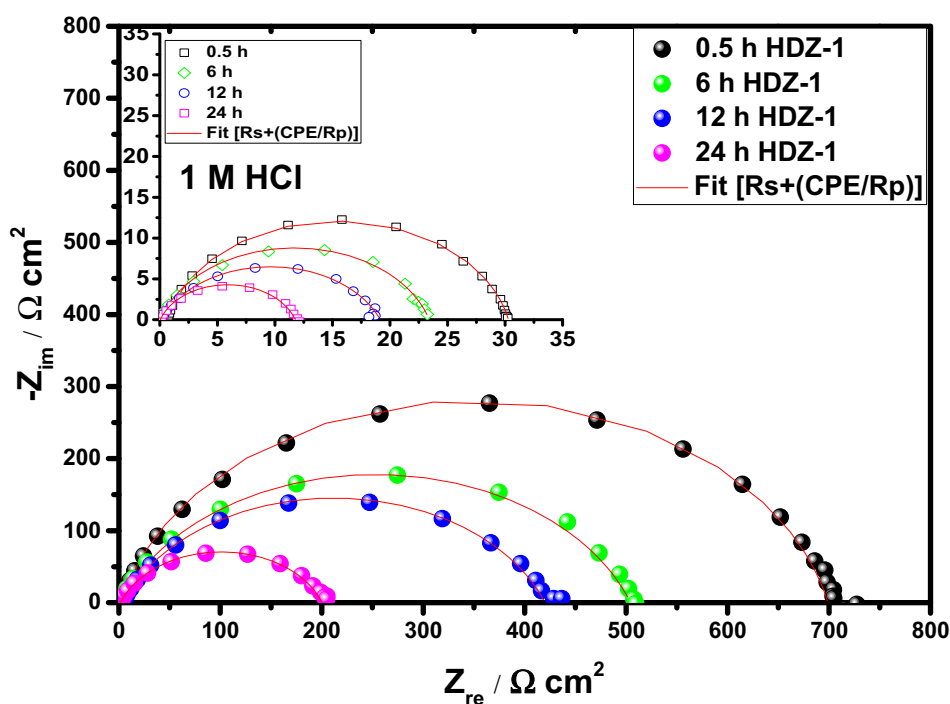


Fig. 3 EIS curves of mild steel substrate immersed in 1 M HCl solution without and with 5×10^{-3} M of HDZ-1 at varied times.

substantial agreement between the inhibition efficiency values from the three tests. Further experimental and theoretical studies were performed to confirm and validate these findings (See sections below).

3.4. Adsorption isotherm

For getting better insights into the nature of adsorption of organic inhibitor molecules on mild steel surface in corrosive

medium, the adsorption isotherms are usually used (Khaled and Abdel-Rehim, 2011; Khaled and El-Maghraby, 2014). Use of such adsorption isotherms can facilitate effective comparison between the inhibitor molecules by fitting the experimentally generated data with isotherm models. The degree of surface coverage (θ) values used for the construction of adsorption isotherm were extracted from weight loss measurements. This is especially important since the immersion time is higher enough to study the adsorption ability of inhibitors.

Table 4 Electrochemical parameters of impedance and inhibition efficiency for mild steel samples in 1 M HCl without and with 5×10^{-3} M of HDZ-1 at varied times.

Inhibitors	Time/h	$R_p^a / \Omega \text{ cm}^2$	n^b	$Q^c \times 10^{-4} / \text{Sn } \Omega^{-1} \text{ cm}^{-2}$	$\chi^2 \times 10^{-3}$	$C_{dl} / \mu\text{F cm}^{-2}$	$\eta_{\text{EIS}} / \%$
Blank	0.5	29.35	0.89	1.7610	0.54	91	–
	6	23.22	0.84	2.5114	2.09	94	–
	12	18.05	0.83	2.9866	2.14	102	–
	24	12.28	0.88	3.0891	4.23	144	–
HDZ-1	0.5	704	0.84	0.2751	2.53	12	95
	6	510	0.86	0.1723	4.01	8	95
	12	436	0.86	0.2007	5.63	9	96
	24	204	0.79	0.4904	1.91	14	94

^a The standard deviation range for R_p : [1.9–6.7%].

^b The standard deviation range for n : [0.8–4.1%].

^c The standard deviation range for Q : [2.3–4.9%].

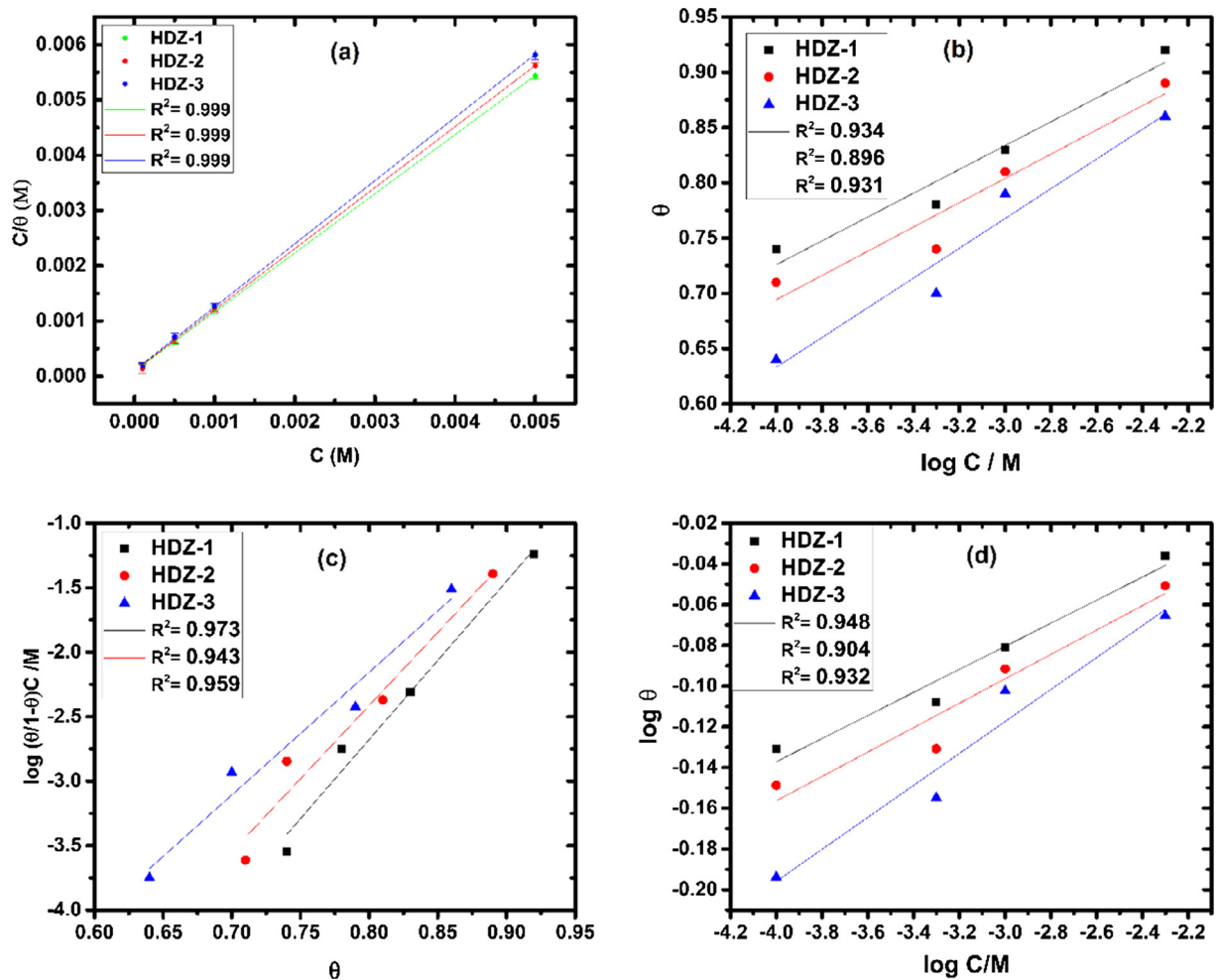


Fig. 4 The isotherm plots for the adsorption of hydrazones on mild steel in 1.0 M HCl at 303 K: (a) Langmuir, (b) Temkin, (c) Frumkin and (d) Freundlich.

The adsorption isotherm was determined by applying different adsorption isotherm models such as Langmuir, Temkin, Freundlich, and Frumkin to the same set of experimental data, where we found that Langmuir model (Fig. 4) serves better

than all the other models. The Langmuir model Eq. (19) is of the following form (Olasunkanmi et al., 2016):

$$\frac{C}{\theta} = \frac{1}{K_{ads}} + C \quad (19)$$

The terms shown in the above equation are defined as follows: K_{ads} is the adsorption-desorption equilibrium constant and C_{inh} is the hydrazones concentration. The $\Delta G_{\text{ads}}^{\circ}$ values (free energy of adsorption) were calculated using the following equation (Olasunkanmi et al., 2016):

$$\Delta G_{\text{ads}}^{\circ} = -RT \ln(K_{\text{ads}} \times C_{\text{solvent}}) \quad (20)$$

where C_{solvent} is the molar concentration of solvent (For H_2O is 55.5 mol L^{-1}).

A correlation between C/θ vs. C (Fig. 4(a)) for three compounds gave a straight line with correlation coefficient (R^2) close to 1, suggesting that the adsorption of tested inhibitors on mild steel surface obeyed the equation of Langmuir's adsorption model.

In addition, it is evident from Table 5 that the slopes of the straight lines are close to 1 which is an indication that there are no interactions among the adsorbed inhibitor molecules.

In an attempt to mitigate the dissolution of mild steel, the inhibitor molecules got adsorbed onto the metal surface by replacing the pre-adsorbed water molecules. The adsorption of inhibitor molecules can be through physical, chemical or physicochemical adsorption. In this regard, the free energy of adsorption can give useful information about the adsorption mode involved in the interaction of hydrazone derivatives to the mild steel surface. According to many authors in the field (Chaitra et al., 2016; Gurudatt and Mohana, 2014), the value of $\Delta G_{\text{ads}}^{\circ} \sim -40 \text{ kJ mol}^{-1}$ or more negative, is mainly counted to be chemisorption, whereas, if $\Delta G_{\text{ads}}^{\circ} \sim -20 \text{ kJ mol}^{-1}$ or less negative, the adsorption is mainly classified as physisorption. In the present study, $\Delta G_{\text{ads}}^{\circ}$ values are in between -20 kJ mol^{-1} and -40 kJ mol^{-1} , which indicate a comprehensive adsorption (both physisorption and chemisorption) (Lgaz et al., 2017b). A better explanation of these results are included in the XPS and theoretical sections.

3.5. XPS studies

In recent years, X-ray photoelectron spectroscopy (XPS) was extensively used in wide range of fields, including material characterization research and surface chemistry of metals (Guzmán et al., 2017). In corrosion inhibition research, XPS is a useful method to ascertain the adsorption of inhibitor molecules on the metal surface (Finšgar and Merl, 2014). The XPS analysis were done on the steel surface after 24 h of immersion time in 1 M HCl solution containing 5×10^{-3} M of HDZ-1 (The three compounds have similar molecular structures and belong to the same family). Fig. 5 shows the obtained high-resolution X-ray photoelectron deconvoluted profiles of Fe $2p_{3/2}$, C 1s, N 1s and O 1s core levels.

Table 5 Adsorption parameters for hydrazone derivatives on mild steel in 1 M HCl at 303 K.

Inhibitor	Slope	K_{ads} (M^{-1})	R^2	$\Delta G_{\text{ads}}^{\circ}$ (kJ mol^{-1})
HDZ-1	1.05	10,696	0.9994	-37.12
HDZ-2	1.07	10,046	0.9996	-36.9
HDZ-3	1.04	9168	0.9998	-36.7

The Fe $2p_{3/2}$ peak for the HDZ-1-treated surface is usually decomposed into four peaks located at ~ 707.0 , ~ 710.5 , ~ 712.2 , and ~ 713.7 eV representing four different environments. The peaks at ~ 710.5 and ~ 712.2 eV are mainly attributed to ferric oxides such as Fe_2O_3 (i.e., Fe^{3+} oxide) and/or Fe_3O_4 (i.e., $\text{Fe}^{2+}/\text{Fe}^{3+}$ mixed oxide) and to ferric hydroxide FeOOH (Bouanis et al., 2009; Pech-Canul and Bartoloperez, 2004), while that located at ~ 707.0 eV is attributable to metallic iron (Di Castro and Ciampi, 1995). The last peak at ~ 713.7 eV may be assigned to the satellite of Fe(III) (Galtayries et al., 2006).

The oxygen 1s X-ray photoelectron spectroscopy (XPS) spectra acquired from mild steel, subsequent to immersion in 1 M HCl solution with HDZ-1 may be fitted into one main peak at ~ 531.8 eV indicating one chemical form of O atom present in the inhibited interface. The peak located at binding energy (~ 531.8 eV) is due to the presence of the oxygen double bonded to carbon ($\text{C}=\text{O}$) (Boyd et al., 2001; Kannan et al., 2007).

The carbon atom based bonds are the main constituent of the inhibitor molecule, thus, the C 1s XPS spectra was recorded in order to get information about the possible chemical forms of C atoms adsorbed on the mild steel surface. The C 1s signal can be deconvoluted in three components located at ~ 285 , ~ 286.4 and ~ 289.2 eV binding energies. The binding energy at ~ 285 eV is consistent with the formation of $\text{C}-\text{C}$, $\text{C}=\text{C}$, and $\text{C}-\text{H}$ bonds related to the different groups of HDZ-1 (Outirite et al., 2010; Seah et al., 1983). It can also be assigned to contaminant hydrocarbons (Bouanis et al., 2016). The C 1s peaks at ~ 286.4 eV could be attributed to the formation of $\text{C}-\text{N}$ and $\text{C}=\text{O}$ groups in hydrazone derivative (Kelemen et al., 2002). The binding energy at ~ 289.2 eV is mainly attributed to the presence of imide group ($\text{N}-\text{C}=\text{O}$) and to the carbon atom of the C^+-O (Briggs and Seah, 2003; Zarrouk et al., 2015) resulting from the protonation of the HDZ-1 molecule in 1 M HCl as shown in the following scheme.

Focusing now on the curve-fitting of the N 1s XPS spectra which can be deconvoluted by using two different components located at 398.8 and 400.2 eV. The binding energy value of 398.8 eV can be assigned to the unprotonated N atoms present in hydrazone group of HDZ-1 while the binding energy of 400.2 eV can be attributed to the coordination of the nitrogen atom with the mild steel surface ($\text{N}-\text{Fe}$) (Tang et al., 2013; Weng et al., 1995).

The inhibition efficiency of HDZ-1 can be enhanced by several ways including chemical and physical interactions. The presence of the heteroatoms such as oxygen and nitrogen in the molecules of hydrazone derivatives facilitates the coordination interaction with iron atoms and leads to a high tendency for protonation in acidic medium. The high amount of π -bonds could definitely enhance the donation via the transfer of electrons from the occupied π orbitals of the inhibitor molecule to iron unoccupied orbitals and back-donation through the transfer of electrons from the d-orbitals of iron to the vacant π^* orbital of the inhibitor molecule. These results are remarkable and highlight the utmost importance of both chemical and physical interactions in enhancing the adsorption of an inhibitor molecule. A fuller picture of these interactions will be developed by combining the experimental data with the results of the theoretical calculations.

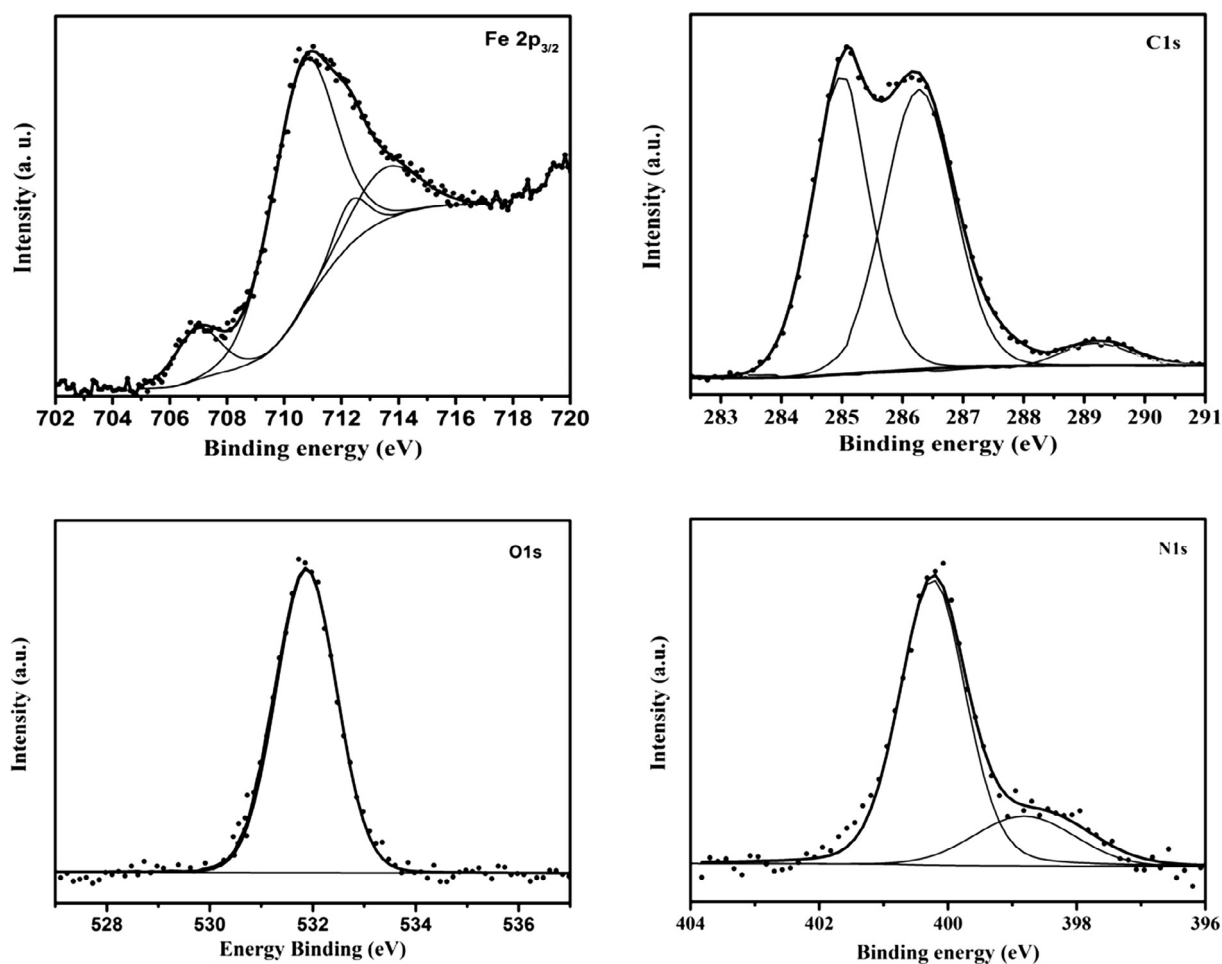


Fig. 5 The XPS deconvoluted profiles of Fe $2p_{3/2}$, C 1s, N 1s and O 1s acquired from mild steel after immersion in 1 M HCl containing 5×10^{-3} M of HDZ-1.

3.6. SEM

SEM pictures were used to further investigate the surface morphology of mild steel before and after 6 h, 12 h and 24 h of immersion in the 1 M HCl solutions with and without 5×10^{-3} M HDZ-1 at 303 K. Fig. 6 shows the surface morphology by SEM for mild steel in absence and presence of tested inhibitor molecule. In absence of inhibitor, it is clearly observed that the surface of the mild steel (after 24 h immersion) is highly corroded and damaged due to rapid corrosion attack in acidic solution. In presence of inhibitor, significant improvements were observed at different immersion times with smoother surfaces. The remarkable improvement of mild steel surface reflects the high adsorption ability of inhibitors on the mild steel surface.

3.7. Quantum chemical calculations

3.7.1. Global reactivity descriptors

In most of the previous corrosion research, Density functional theory (DFT) calculations played a major role in predicting the adsorption ability of inhibitors through the successful investigation of their electronic properties (Guo et al., 2017).

In the light of this, and as a continuation of our efforts towards understanding factors that affect the effectiveness of tested hydrazone derivatives, quantum chemical calculations were performed using density functional theory (DFT) methodology. Fig. 7 shows the fully optimized geometries, HOMO called as the highest occupied molecular orbital, LUMO called as the lowest unoccupied molecular orbital and molecular electrostatic potential (MEP) of the three inhibitors molecules.

The reactive sites of the molecules can be better studied by analyzing the HOMO and LUMO while the reactivity trend can be identified by studying the electronic parameters. The electron donation tendency of a compound is mainly associated with an increase in HOMO energy whereas the electron acceptance ability is correlated with a decrease of LUMO energy (Singh et al., 2018). Fig. 7 shows that the HOMO is partially distributed on the molecular structure of the HDZ-2 and HDZ-3 without any observed reactivity of substituted phenyl. It is also evident that both inhibitors have similar HOMO distribution while in HDZ-1, the electron density has extended on almost the entire molecular structure, thereby enhancing the donating ability of this compound. Besides, the insignificant HOMO densities on the C=O group is because oxygen atom has higher electronegativity and therefore it has

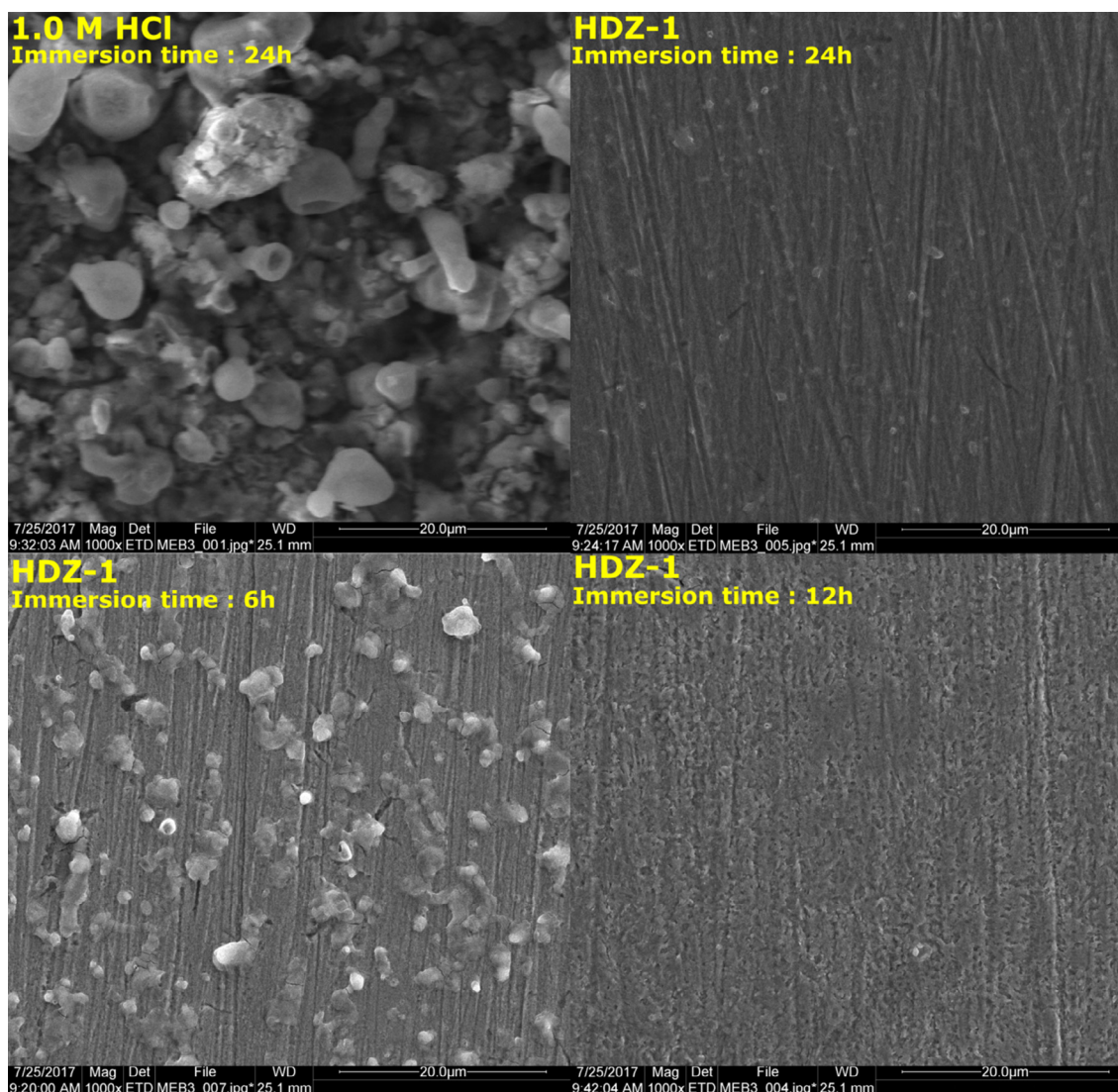


Fig. 6 SEM micrographs acquired from mild steel samples subsequent to immersion for 6, 12 and 24 h in 1 M HCl at 303 K.

greater tendency to hold onto its lone pair of electrons. On the other hand, the LUMO electron densities of HDZ-2 and HDZ-3 shifted toward the non-reactive parts in HOMO distributions. In return, like HOMO distribution, the LUMO electron density of HDZ-1 is localized almost on the entire molecular structure showing the tendency of the mentioned compound towards chemical and physical interactions, which further support the experimental investigations.

Table 6 reports the quantum chemical parameters, i.e. HOMO and LUMO energies, HOMO–LUMO gaps ($\Delta E = E_{\text{HOMO}} - E_{\text{LUMO}}$) and fraction of electron transferred ΔN . The HOMO energy corresponds to the ability of an inhibitor molecule to offer electrons to another molecule having empty orbitals (Saha et al., 2016). A high value of HOMO energy for a molecule is related to its tendency to donate electrons to the vacant orbital of the metal atoms while a decrease in LUMO energy reflects the ease of electron acceptance by this level (Saha et al., 2016). The energy gap is one of the key quantum chemical parameters in a comparison between inhibitor molecules having similar molecular structures since it charac-

terizes the chemical reactivity, molecular chemical stability, and hardness of an inhibitor molecule. The adsorption ability, thus the inhibition performance increases when ΔE_{gap} value decreases, whereas a higher value of energy gap is associated with high stability of the compound, thus a low tendency to react (Singh et al., 2016). It is apparent from Table 6 that the inhibitor molecule possessing the highest E_{HOMO} value is HDZ-1, followed by HDZ-2 while the HDZ-3 has the lowest HOMO value. The extent to which the molecule can accept electrons is indicated by E_{LUMO} values. Thus, compared to HDZ-2 and HDZ-3, the inhibitor molecule HDZ-1 has a greater tendency towards electron donation to iron atoms. As follows from Table 6, the extent of increment for the LUMO energies follows the order of $\text{HDZ-2} < \text{HDZ-3} < \text{HDZ-1}$ which is not in agreement with the order of the inhibition efficiency. As reported in Table 6, the HDZ-1 possesses the lowest energy gap, followed by HDZ-2 while the HDZ-3 has the higher energy gap value following therefore the order of corresponding inhibition efficiency. Previous experimental and theoretical studies had noted that there is a good correla-

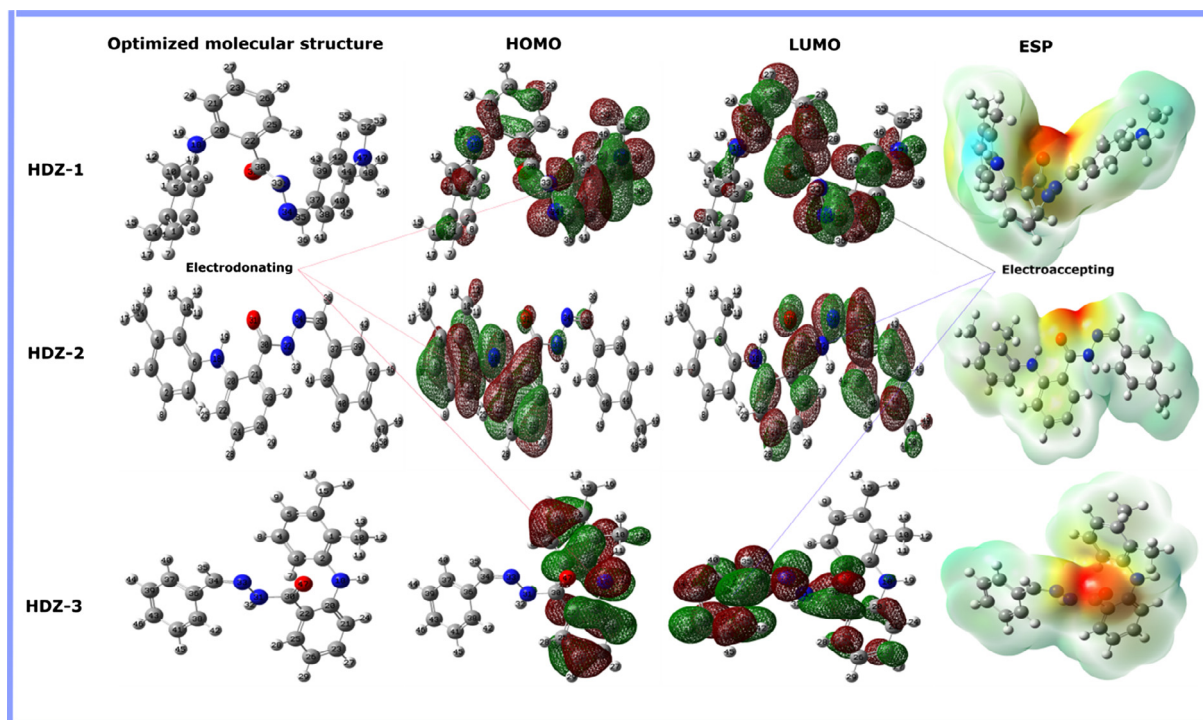


Fig. 7 Optimized molecular structure, HOMO and LUMO orbitals, and molecular electrostatic potential of hydrazone derivatives calculated at DFT/6-311++G(d, p).

Table 6 Calculated Quantum chemical parameters for hydrazone derivatives obtained from DFT/B3LYB/6-311++G(d, p).

Inhibitors	E_{HOMO} (eV)	E_{LUMO} (eV)	ΔE_{gap} (eV)	ΔN_{110}
HDZ-1	-4.410	-0.815	3.595	0.162
HDZ-2	-5.055	-1.433	3.622	0.104
HDZ-3	-5.219	-1.317	3.902	0.095

tion between the amount of electron transferred from the inhibitor to metal atoms and the strength of the interactions between inhibitor and metal surface. It is noted that an inhibitor molecule transfer its electrons to metal if $\Delta N > 0$ and vice versa if $\Delta N < 0$ (Kokalj, 2010; Kovačević and Kokalj, 2011). Therefore, according to this criterion, the results in Table 6 show that the three compounds have the tendency to donate electrons to the metal surface. In addition, the ΔN values follow the same order of the HOMO energies values, which indicate that the electron donating ability of the inhibitor molecules plays the crucial role in the difference between tested compounds. The results emerged from the quantum chemical parameters somewhat match and confirm those obtained from XPS studies which show that the potential sites for electron donation are more dominant than those of electron acceptance.

3.7.2. Molecular electrostatic potential (MEP)

The MEP is an important informative property for identifying the highest and lowest electron density regions in an inhibitor molecule (Rahmani et al., 2018). The MEP maps have been extracted after completing geometry optimization using the

Gaussian program (Fig. 7). The MEP maps were evaluated by considering the values of the electrostatic potential. The red color stands for the regions of the most negative MEP while the blue color shows the regions of the most positive, and green for zero MEP (Ramalingam et al., 2011). Thus, the potential decreases following the order of: blue > green > yellow > orange > red. In the MEP maps above, it is evident that the most electrostatic potential indicated by deep red color is concentrated around the C=O group which suggest a deficiency of electrons and therefore a possible center for physical adsorption via electrostatic interaction. The other parts of the molecules are mainly associated with nucleophilic reactivity or a potential halfway between red and blue color.

3.7.3. Fukui functions

From the results mentioned above, it can be concluded that the hydrazone derivatives possess higher susceptibility to accepting and donating electrons from/to iron atoms. Thus, the identification of the most reactive sites may be very useful in supporting experimental-based hypothesis. To this end, the condensed Fukui functions of the inhibitor molecule can be a useful parameters in assessing the local reactivity of the inhibitor molecules (Lgaz et al., 2017a).

The local reactivity analysis based on the Fukui function calculations provides information about the atomic site with the highest tendency to be involved in electrophilic and nucleophilic reactions. The atomic sites for electrophilic will be those bearing a positive charge (f^+) and possessing a tendency to accept an electron while those for nucleophilic bearing a negative charge (f^-) and possessing a tendency to donate an electron (Lgaz et al., 2017b). The greater the Fukui function value of a given atom is, the higher its local reactivity (Lgaz

et al., 2017b). The most active sites for nucleophilic and electrophilic attacks are graphically represented in Fig. 8.

In the HDZ-1, most positive atoms of f^- function are located on the N(34), C(37), and N(47); while most positive atoms of f^+ function are located on the C(23), O(31) and C(38). In HDZ-2, the most positive atoms of f^- function are located on C(4), C(14) and C(26); while most positive atoms of f^+ function are located on the N(18), N(34) and C(35). In

the case of HDZ-3, N(18), C(21) and C(26) are the most positive atoms of f^- while C(30), C(34), and C(43) are the most electrophilic sites. Overall, these results are generally reassuring since there is a clear trend in increasing electro-donating tendency from HDZ-3 to HDZ-1. It can be also observed that the electron donation ability seems to be more important than that of electron acceptance, which well supports the above-mentioned results.

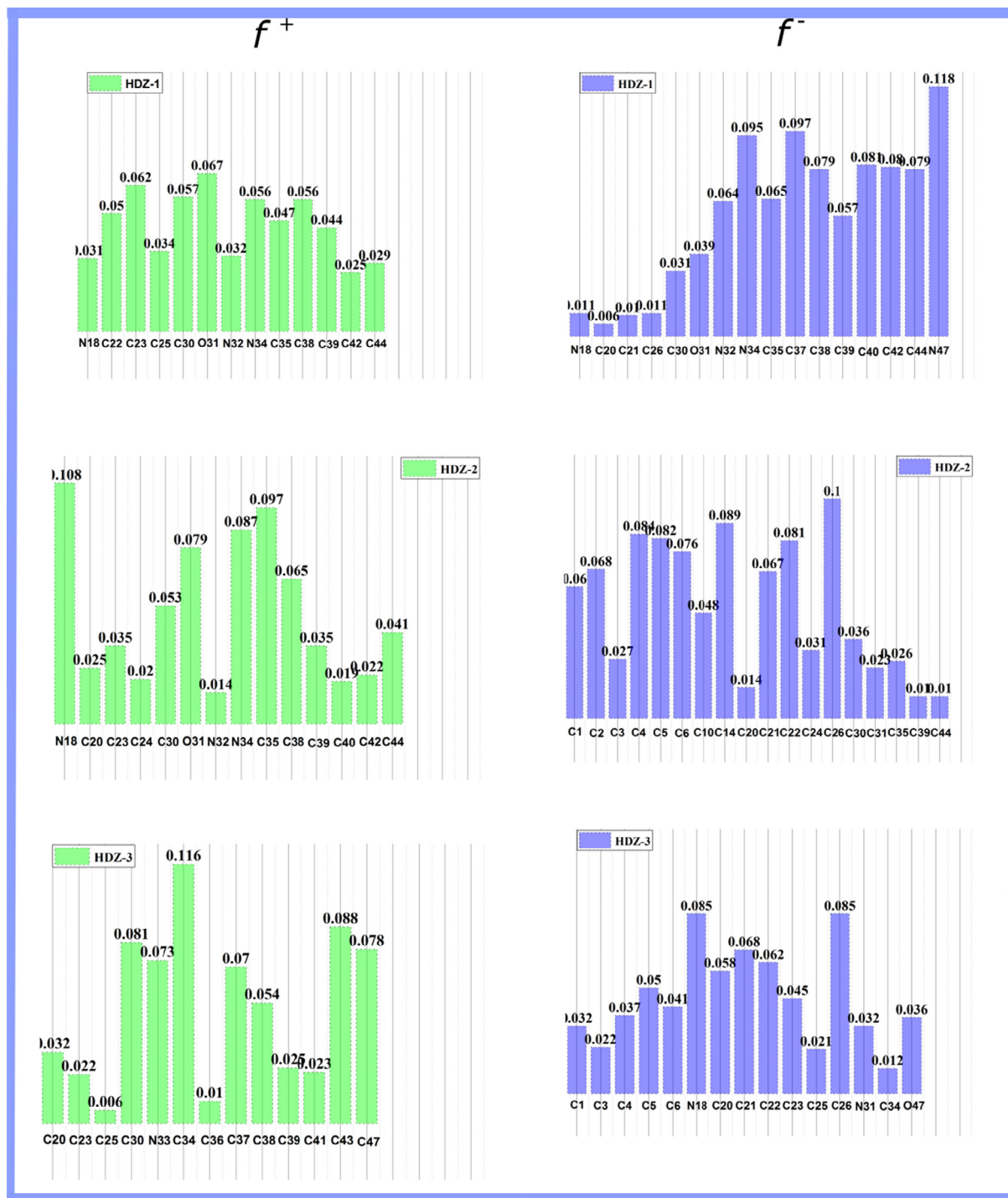


Fig. 8 Graphical representation of the calculated Fukui indices of hydrazone derivatives.

3.8. MD simulations

With increasing computational power and memory, the use of computational techniques holds a great promise to provide accurate simulations for more complex physicochemical systems. In recent years, there has been growing interest in the use of molecular dynamics (MD) simulations to study the movement of atoms directly (Ricke, 2018; Wypych, 2017). In corrosion research field, one of the recent themes is the understanding of the corrosion inhibition process at an atomic or molecular level (Weder et al., 2016). In the light of this, and as a continuation of our efforts towards a more comprehensive evaluation of the corrosion inhibition properties of tested organic compounds, MD simulations have been done on an inhibitor and its environment of solvent and corrosive particles like H_3O^+ and Cl^- ions.

Fig. 9 presents the best adsorption configuration of the tested inhibitors on the Fe(1 1 0) surface. Careful inspection of this figure reveals that the studied molecules move to the Fe (1 1 0) surface to parallel or flat disposition. Without a doubt, the flat disposition of inhibitors can play an essential role during adsorption on the surface of the metal since corrosion inhibitors with parallel adsorption have better chances of covering a wide area of the metal surface, thus great extent of inhibition efficiency. The extent of interaction between the Fe surface and inhibitor molecules can unambiguously be demonstrated by estimating the interaction and binding energies. A large negative values of the interaction energies indicates that the interactions between inhibitor molecules and Fe(1 1 0) surface are strong (Zhou et al., 2008). As Table 7 shows, there is a significant difference between three simulated compounds, the HDZ-1 has the highest absolute value of interaction energy, followed by HDZ-2; and the lowest value is for HDZ-3. Therefore, It can be confirmed that the increase of the interaction

Table 7 Output obtained from MD simulation for adsorption of hydrazone derivatives on Fe (1 1 0) surface.

System	$E_{\text{interaction}}$ (kJ/mol)	E_{binding} (kJ/mol)
Fe(110) + HDZ-1	-619.91	619.91
Fe(110) + HDZ-2	-491.53	491.53
Fe(110) + HDZ-3	-401.88	401.88

energy depend on the nature of electron donating groups. Furthermore, it is noteworthy that high binding energy implies that the adsorption of inhibitor molecules is strong and stable on Fe(1 1 0) surface (Obot et al., 2013; Zhou et al., 2008). In this context, Anton Kokalj in his comments on the paper by Mendes et al. (Mendes et al., 2012) has written that higher magnitude of binding energy indicates that probably there is more than one bond to the surface per molecule (Kokalj, 2013). Even though the changes between inhibitor molecules were small from a molecular point of view, the inhibitor with $-N(CH_3)_2$ group has more tendency to interact with the metal surface, hence, increasing the inhibition efficiency due to high electron donating property of this group (Singh et al., 2018). Thus, a change in structure, and/or in the nature of the functional group, is expected to affect the compound's efficiency. Our results are in good agreement with experimental and DFT calculations and broadly supported the majority of the findings in the literature.

3.9. Radial distribution function

To further explore the interaction mechanism between inhibitor molecules and iron atoms, radial distribution functions were analyzed from MD trajectories. The RDF is an

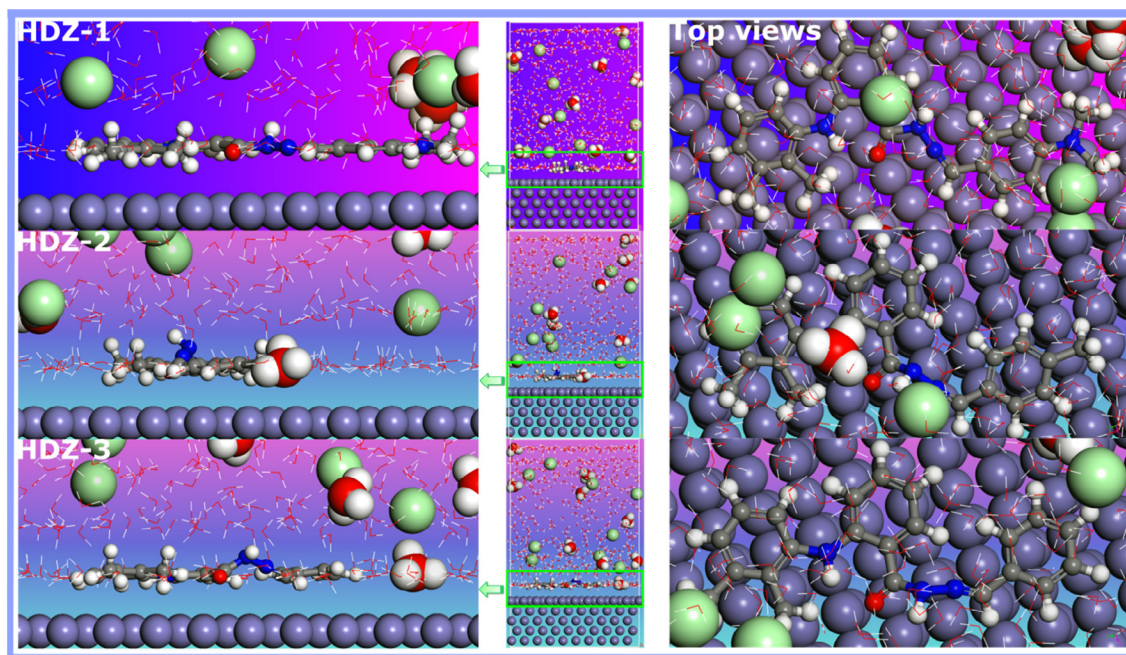


Fig. 9 Equilibrium adsorption configurations of the hydrazone derivatives on the Fe (1 1 0) surface in solution obtained by molecular dynamics simulations.

advantageous technique to determine the bond length and its peak distance indicate how much meaningful are interactions of inhibitor molecules with iron surface (Benzon et al., 2017). Particularly, the typical bond length of physisorption is greater than 3.5 \AA , much longer than chemical interaction types, which fall in the range of 1 \AA – 3.5 \AA (Xie et al., 2015). The total radial distribution functions of all inhibitor molecules are represented in Fig. 10.

From the data in Fig. 10, it is apparent that all inhibitor molecules have interesting interaction with iron atoms. The first peaks for (HDZ-3)-Fe, (HDZ-2)-Fe and (HDZ-1)-Fe are

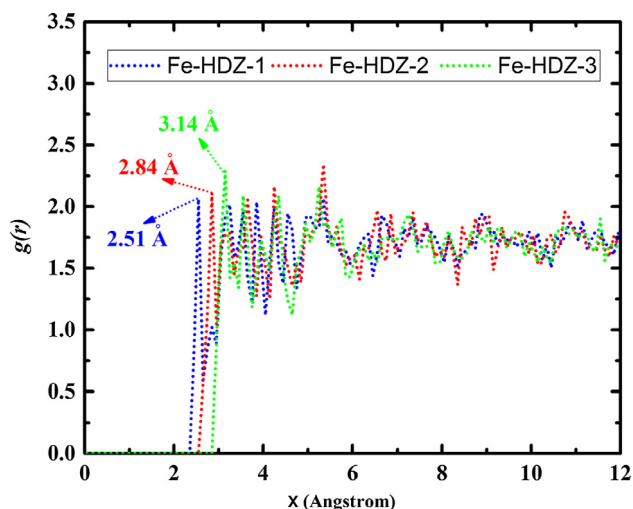


Fig. 10 RDF analysis of hydrazone derivatives adsorbed on the Fe (1 1 0) surface in solution.

all located at distances smaller than 3.5 \AA . The functional groups that include heteroatoms and π -electrons provide key interactive force to inhibitor molecules. Like experimental and quantum chemical calculations results, the RDFs results show strikingly similar extent of adsorption where the HDZ-1 has the strongest interactions with iron atoms. The results of RDFs indicate that the interactive forces were also well correlated with the order of the binding energies. In summary, these results provide strong evidence for the effect of the functional groups, especially those with significant electro-donating properties, on the inhibitive performance of organic compounds.

3.10. Anticorrosion mechanism of hydrazone derivatives

Although there are a large number of published studies reporting various biological properties of hydrazone derivatives, the studies on the effectiveness and mechanism of these compounds in corrosion inhibition remain insufficient. Herein, the results showed that the hydrazone derivatives are effective corrosion inhibitors with great electronic properties. The Tafel polarization results showed that the three compounds are mixed type inhibitors controlling both anodic and cathodic reactions. The electrochemical and weight loss data showed that corrosion resistance of mild steel in presence of HDZ-1 is evidently superior to those with HDZ-2 and HDZ-3. In addition to experimental data, the computational calculations provided a great help in explaining the adsorption strength of inhibitors and identifying the active sites. It was expected that the investigated compounds would markedly reduce the corrosion rate of mild steel owing to their unique chemical reactivity. The presence of nitrogen and oxygen atoms allows the hydrazones to exhibit both hard and soft base characters

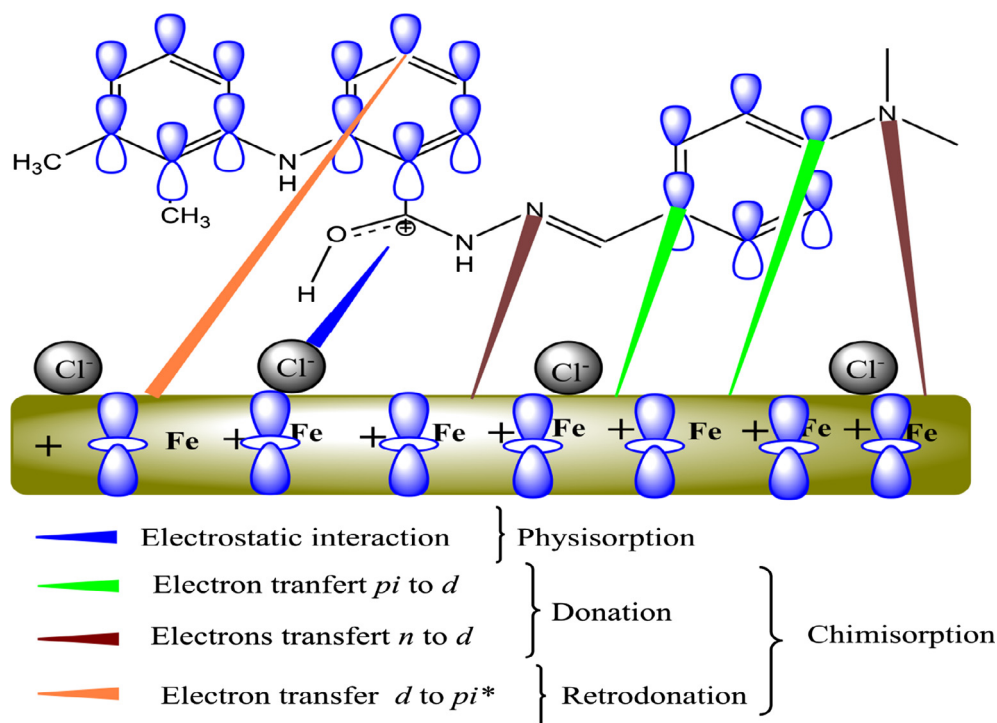


Fig. 11 Pictorial representation of adsorption of HDZ-1 on mild steel surface in 1 M HCl solution.

and thus leads to a strong interaction with the steel surface. This statement was supported by XPS studies, which showed that the HDZ-1 is mainly chemically adsorbed on the steel surface along with, to some extent, the existing physical adsorption. Furthermore, the difference in inhibition efficiency between HDZ-1 and unsubstituted HDZ-3 was significant. The possible reason for this result was found to be due to the electron donating power of $(-N(CH_3)_2)$. As the observed outcome of the present investigation, which represents a combination of a multitude of interactions between studied hydrazones and mild steel surface, we can suggest that the inhibition mechanism is mainly a result of a combination of a three kinds of interactions (Fig. 11):

- (I) The surface charge of the mild steel plays a crucial role during interaction with an inhibitor molecule. It is consistently seen in similar studies (Yildiz et al., 2014) that the mild steel surface carries a positive excess charge in HCl solution. Moreover, it is known that organic inhibitor molecules having heteroatoms in their molecular structure are expected to be protonated in an acidic solution in balance with the matching molecular structure (Yildiz et al., 2014). Therefore, the chlorine ions will be preferentially adsorbed onto the steel surface, thus, permit positively charged HDZs to come into negatively charged metal surface through the formation of electrostatic interactions (Solmaz et al., 2008).
- (II) The physical adsorption is the first step and the base of chemical adsorption, then, the hydrazone derivatives can be chemically adsorbed through acceptor-donor interactions (Tang et al., 2006). The presence of π electrons of the phenyl rings and unshared electron pairs in heteroatoms can ensure the donation of the electron to the vacant d-orbitals of iron, which is chemical adsorption.
- (III) A greater amount of reactive sites might leads to an extra negative charge on steel surface due to a strong donation of electrons. This extra charge might be transferred to inhibitor molecules by means of back-donation interactions, which mean the transfer of electrons from the d-orbitals of iron to the vacant π^* orbital of the inhibitor molecules.

4. Conclusion

The present study was designed to determine the inhibitive effect of three hydrazone derivatives, HDZ-1, HDZ-2, and HDZ-3 on the corrosion of mild steel in 1 M HCl using a combined experimental and theoretical approach. Among the tested compounds, the HDZ-1 produces the better inhibitive performances with inhibition efficiency (95%) higher than HDZ-2 (90%) and HDZ-3 (84%). The electrochemical results illustrate that the HDZs behave as mixed type inhibitors; their addition to corrosive solutions leads to a high increase of the polarization resistance and correspondingly lower double-layer capacitance. The information about adsorption mode was extracted from Langmuir adsorption model. A simultaneous donation and retrodonation of electrons were proposed as a mode of interaction between the hydrazone derivatives and iron atoms with higher contribution of electron donating

effect. XPS methods, molecular dynamics simulations, DFT and radial distribution function were used to ascertain the adsorption mode of the hydrazone derivatives on the mild steel surface. Synergistic chemical and physical interactions were well supported by theoretical studies. The insights gained from these studies are very important for us, so we can continue to invest in the development of more efficient corrosion inhibitors through functionalization of others NSAID's.

Acknowledgments

This paper was supported by Konkuk University Researcher Fund in 2017.

References

- Abdel-Rehim, S.S., Khaled, K.F., Al-Mobarak, N.A., 2011. Corrosion inhibition of iron in hydrochloric acid using pyrazole. *Arab. J. Chem.* 4, 333–337. <https://doi.org/10.1016/j.arabj.2010.06.056>.
- Abdul Rahiman, A.F.S., Sethumanickam, S., 2017. Corrosion inhibition, adsorption and thermodynamic properties of poly(vinyl alcohol-cysteine) in molar HCl. *Arab. J. Chem.* 10, S3358–S3366. <https://doi.org/10.1016/j.arabj.2014.01.016>.
- Alibakhshi, E., Ramezanzadeh, M., Bahlakeh, G., Ramezanzadeh, B., Mahdavian, M., Motamedi, M., 2018. Glycyrrhiza glabra leaves extract as a green corrosion inhibitor for mild steel in 1 M hydrochloric acid solution: experimental, molecular dynamics, Monte Carlo and quantum mechanics study. *J. Mol. Liq.* 255, 185–198.
- Almasirad, A., Tajik, M., Bakhtiari, D., Shafiee, A., Abdollahi, M., Zamani, M.J., Khorasani, R., Esmaily, H., 2005. Synthesis and analgesic activity of N-arylhydrazone derivatives of mefenamic acid. *J. Pharm. Pharm. Sci.* 8, 419–425.
- Antonio, M., Maggio, R.M., 2018. Assessment of mefenamic acid polymorphs in commercial tablets using chemometric coupled to MIR and NIR spectroscopies. Prediction of dissolution performance. *J. Pharm. Biomed. Anal.* 149, 603–611.
- Aronson, J.K. (Ed.), 2016. Mefenamic acid, in: Meyler's Side Effects of Drugs, sixteenth ed. Elsevier, Oxford, pp. 787–789. <https://doi.org/10.1016/B978-0-444-53717-1.01027-1>.
- ASTM Committee G-1 on Corrosion of Metals, 2011. Standard practice for preparing, cleaning, and evaluating corrosion test specimens. ASTM International.
- Becke, A.D., 1988. Density-functional exchange-energy approximation with correct asymptotic behavior. *Phys. Rev. A* 38, 3098–3100. <https://doi.org/10.1103/PhysRevA.38.3098>.
- Bentiss, F., Gassama, F., Barbry, D., Gengembre, L., Vezin, H., Lagrenée, M., Traisnel, M., 2006. Enhanced corrosion resistance of mild steel in molar hydrochloric acid solution by 1,4-bis(2-pyridyl)-5H-pyridazino[4,5-b]indole: Electrochemical, theoretical and XPS studies. *Appl. Surf. Sci.* 252, 2684–2691. <https://doi.org/10.1016/j.apsusc.2005.03.231>.
- Benzon, K., Mary, Y.S., Varghese, H.T., Panicker, C.Y., Armaković, S., Armaković, S.J., Pradhan, K., Nanda, A.K., Van Alsenoy, C., 2017. Spectroscopic, DFT, molecular dynamics and molecular docking study of 1-butyl-2-(4-hydroxyphenyl)-4, 5-dimethyl-imidazole 3-oxide. *J. Mol. Struct.* 1134, 330–344.
- Bouanis, F., Bentiss, F., Traisnel, M., Jama, C., 2009. Enhanced corrosion resistance properties of radiofrequency cold plasma nitrated carbon steel: gravimetric and electrochemical results. *Electrochim. Acta* 54, 2371–2378.
- Bouanis, M., Tourabi, M., Nyassi, A., Zarrouk, A., Jama, C., Bentiss, F., 2016. Corrosion inhibition performance of 2, 5-bis (4-dimethylaminophenyl)-1, 3, 4-oxadiazole for carbon steel in HCl solution: Gravimetric, electrochemical and XPS studies. *Appl. Surf. Sci.* 389, 952–966.

- Boyd, R.D., Verran, J., Hall, K.E., Underhill, C., Hibbert, S., West, R., 2001. The cleanability of stainless steel as determined by X-ray photoelectron spectroscopy. *Appl. Surf. Sci.* 172, 135–143. [https://doi.org/10.1016/S0169-4332\(00\)00840-0](https://doi.org/10.1016/S0169-4332(00)00840-0).
- Briggs, D., Seah, M., 2003. *Practical surface analysis: by auger and x-ray photoelectron spectroscopy*. Wiley.
- Cao, Z., Tang, Y., Cang, H., Xu, J., Lu, G., Jing, W., 2014. Novel benzimidazole derivatives as corrosion inhibitors of mild steel in the acidic media. Part II: Theoretical studies. *Corros. Sci.* 83, 292–298.
- Chaitra, T.K., Mohana, K.N., Gurudatt, D.M., Tandon, H.C., 2016. Inhibition activity of new thiazole hydrazones towards mild steel corrosion in acid media by thermodynamic, electrochemical and quantum chemical methods. *J. Taiwan Inst. Chem. Eng.* 67, 521–531. <https://doi.org/10.1016/j.jtice.2016.08.013>.
- Chidiebere, M.A., Oguzie, E.E., Liu, L., Li, Y., Wang, F., 2014. Corrosion inhibition of Q235 mild steel in 0.5 M H₂SO₄ solution by phytic acid and synergistic iodide additives. *Ind. Eng. Chem. Res.* 53, 7670–7679. <https://doi.org/10.1021/ie404382v>.
- Di Castro, V., Ciampi, S., 1995. XPS study of the growth and reactivity of FeMnO thin films. *Surf. Sci.* 331, 294–299.
- Dwivedi, D., Lepková, K., Becker, T., 2017. Carbon steel corrosion: a review of key surface properties and characterization methods. *RSC Adv.* 7, 4580–4610. <https://doi.org/10.1039/C6RA25094G>.
- El Azhar, M., Mernari, B., Traisnel, M., Bentiss, F., Lagrenee, M., 2001. Corrosion inhibition of mild steel by the new class of inhibitors [2, 5-bis (n-pyridyl)-1, 3, 4-thiadiazoles] in acidic media. *Corros. Sci.* 43, 2229–2238.
- El Mehdi, B., Mernari, B., Traisnel, M., Bentiss, F., Lagrenee, M., 2003. Synthesis and comparative study of the inhibitive effect of some new triazole derivatives towards corrosion of mild steel in hydrochloric acid solution. *Mater. Chem. Phys.* 77, 489–496.
- Esmaili, N., Neshati, J., Yavari, I., 2015. Corrosion inhibition of new thiocarbonylhydrazides on the carbon steel in hydrochloric acid solution. *J. Ind. Eng. Chem.* 22, 159–163. <https://doi.org/10.1016/j.jiec.2014.07.004>.
- Feng, L., Zhang, S., Qiang, Y., Xu, S., Tan, B., Chen, S., 2018. The synergistic corrosion inhibition study of different chain lengths ionic liquids as green inhibitors for X70 steel in acidic medium. *Mater. Chem. Phys.* 215, 229–241.
- Finšgar, M., Merl, D.K., 2014. An electrochemical, long-term immersion, and XPS study of 2-mercaptobenzothiazole as a copper corrosion inhibitor in chloride solution. *Corros. Sci.* 83, 164–175.
- Fouda Abd El-Aziz, S., Al-Sarawy, Ahmed A., Radwan, Mohamed S., 2006. Some aromatic hydrazone derivatives as inhibitors for the corrosion of C-steel in phosphoric acid solution. *Ann. Chim.* 96, 85–96. <https://doi.org/10.1002/adic.200690009>.
- Frisch, M., Trucks, G., Schlegel, H., Scuseria, G., Robb, M., Cheeseman, J., Zakrzewski, V., Montgomery Jr, J., Stratmann, R., Burant, J., 2009. Gaussian 09, Gaussian, Inc., Pittsburgh, PA; (b) Dalton 2.0 Program Package (n.d).
- Galtayries, A., Warocquier-Clerout, R., Nagel, M., Marcus, P., 2006. Fibronectin adsorption on Fe–Cr alloy studied by XPS. *Surf. Interface Anal.* 38, 186–190.
- Gholami, M., Danaee, I., Maddahy, M.H., RashvandAvei, M., 2013. Correlated ab initio and electroanalytical study on inhibition behavior of 2-mercaptobenzothiazole and its thiole–thione tautomerism effect for the corrosion of steel (API 5L X52) in sulphuric acid solution. *Ind. Eng. Chem. Res.* 52, 14875–14889.
- Guo, L., Ren, X., Zhou, Y., Xu, S., Gong, Y., Zhang, S., 2017. Theoretical evaluation of the corrosion inhibition performance of 1,3-thiazole and its amino derivatives. *Arab. J. Chem.* 10, 121–130. <https://doi.org/10.1016/j.arabjc.2015.01.005>.
- Gurudatt, D.M., Mohana, K.N., 2014. Synthesis of new pyridine based 1,3,4-oxadiazole derivatives and their corrosion inhibition performance on mild steel in 0.5 M hydrochloric acid. *Ind. Eng. Chem. Res.* 53, 2092–2105. <https://doi.org/10.1021/ie402042d>.
- Guzmán, H.J., Isquierdo, F., Carbognani, L., Vitale, G., Scott, C.E., Pereira-Almao, P., 2017. X-ray photoelectron spectroscopy analysis of hydrotreated athabasca asphaltenes. *Energy Fuels* 31, 10706–10717. <https://doi.org/10.1021/acs.energyfuels.7b01863>.
- Hegazy, M., Badawi, A., El Rehim, S.A., Kamel, W., 2013. Corrosion inhibition of carbon steel using novel N-(2-(2-mercaptoacetoxy) ethyl)-N, N-dimethyl dodecan-1-aminium bromide during acid pickling. *Corros. Sci.* 69, 110–122.
- Joo, Y., Kim, H.-S., Woo, R.-S., Park, C.H., Shin, K.-Y., Lee, J.-P., Chang, K.-A., Kim, S., Suh, Y.-H., 2006. Mefenamic acid shows neuroprotective effects and improves cognitive impairment in in vitro and in vivo Alzheimer's disease models. *Mol. Pharmacol.* 69, 76–84.
- Kannan, A.G., Choudhury, N.R., Dutta, N.K., 2007. Synthesis and characterization of methacrylate phospho-silicate hybrid for thin film applications. *Polymer* 48, 7078–7086.
- Kelemen, S., Afeworki, M., Gorbaty, M., Cohen, A., 2002. Characterization of organically bound oxygen forms in lignites, peats, and pyrolyzed peats by X-ray photoelectron spectroscopy (XPS) and solid-state ¹³C NMR methods. *Energy Fuels* 16, 1450–1462.
- Khaled, K.F., Abdel-Rehim, S.S., 2011. Electrochemical investigation of corrosion and corrosion inhibition of iron in hydrochloric acid solutions. *Arab. J. Chem.* 4, 397–402. <https://doi.org/10.1016/j.arabjc.2010.07.006>.
- Khaled, K.F., El-Maghraby, A., 2014. Experimental, Monte Carlo and molecular dynamics simulations to investigate corrosion inhibition of mild steel in hydrochloric acid solutions. *Arab. J. Chem.* 7, 319–326. <https://doi.org/10.1016/j.arabjc.2010.11.005>.
- Kokalj, A., 2013. Comments on the “Reply to comments on the paper ‘On the nature of inhibition performance of imidazole on iron surface’” by JO Mendes and AB Rocha. *Corros. Sci.* 70, 294–297.
- Kokalj, A., 2012. On the HSAB based estimate of charge transfer between adsorbates and metal surfaces. *Chem. Phys.* 393, 1–12.
- Kokalj, A., 2010. Is the analysis of molecular electronic structure of corrosion inhibitors sufficient to predict the trend of their inhibition performance. *Electrochim. Acta* 56, 745–755.
- Kovačević, N., Kokalj, A., 2011. Analysis of molecular electronic structure of imidazole-and benzimidazole-based inhibitors: a simple recipe for qualitative estimation of chemical hardness. *Corros. Sci.* 53, 909–921.
- Laamari, M.R., Benzakour, J., Berrekhis, F., Derja, A., Villemin, D., 2016. Adsorption and corrosion inhibition of carbon steel in hydrochloric acid medium by hexamethylenediamine tetra(methylene phosphonic acid). *Arab. J. Chem.* 9, S245–S251. <https://doi.org/10.1016/j.arabjc.2011.03.018>.
- Lee, C., Yang, W., Parr, R.G., 1988. Development of the Colle-Salvetti correlation-energy formula into a functional of the electron density. *Phys. Rev. B* 37, 785–789. <https://doi.org/10.1103/PhysRevB.37.785>.
- Lgaz, H., Salghi, R., Subrahmanya Bhat, K., Chaouiki, A., Shubhalaxmi, Jodeh, S., 2017a. Correlated experimental and theoretical study on inhibition behavior of novel quinoline derivatives for the corrosion of mild steel in hydrochloric acid solution. *J. Mol. Liq.* 244, 154–168. <https://doi.org/10.1016/j.molliq.2017.08.121>.
- Lgaz, H., Subrahmanya Bhat, K., Salghi, R., Shubhalaxmi, Jodeh, S., Algarra, M., Hammouti, B., Ali, I.H., Essamri, A., 2017b. Insights into corrosion inhibition behavior of three chalcone derivatives for mild steel in hydrochloric acid solution. *J. Mol. Liq.* 238, 71–83. <https://doi.org/10.1016/j.molliq.2017.04.124>.
- Luo, X., Pan, X., Yuan, S., Du, S., Zhang, C., Liu, Y., 2017. Corrosion inhibition of mild steel in simulated seawater solution by a green eco-friendly mixture of glucomannan (GL) and bisquaternary ammonium salt (BQAS). *Corros. Sci.* 125, 139–151.
- Martinez, S., 2003. Inhibitory mechanism of mimosa tannin using molecular modeling and substitutional adsorption isotherms. *Mater. Chem. Phys.* 77, 97–102.
- Materials Studio, 2013. Revision 6.0. Accelrys Inc., San Diego, USA.

- Mehdipour, M., Ramezanzadeh, B., Arman, S., 2015. Electrochemical noise investigation of Aloe plant extract as green inhibitor on the corrosion of stainless steel in 1 M H₂SO₄. *J. Ind. Eng. Chem.* 21, 318–327.
- Mendes, J.O., da Silva, E.C., Rocha, A.B., 2012. On the nature of inhibition performance of imidazole on iron surface. *Corros. Sci.* 57, 254–259.
- Mendoza, A., Meléndrez-Luevano, R., Cabrera-Vivas, B.M., Lozano-Márquez, C.D., Carranza, V., 2012. (E)-1-Benzyl-idene-2,2-diphenyl-hydrazine. *Acta Crystallogr. Sect. E Struct. Rep Online* 68, o434. <https://doi.org/10.1107/S1600536812000657>.
- Mi, H., Xiao, G., Chen, X., 2015. Theoretical evaluation of corrosion inhibition performance of three antipyrine compounds. *Comput. Theor. Chem.* 1072, 7–14. <https://doi.org/10.1016/j.comptc.2015.08.023>.
- Mohamed, S.K., Mague, J.T., Akkurt, M., Mohamed, A.F., Albayati, M.R., 2015. Crystal structure of 2-(2, 3-dimethylanilino)-N'-[(1E)-2-hydroxybenzylidene] benzohydrazide. *Acta Crystallogr. Sect. E Crystallogr. Commun.* 71, o957–o958.
- Obot, I., Obi-Egbedi, N., Ebenso, E., Afolabi, A., Ogunzue, E., 2013. Experimental, quantum chemical calculations, and molecular dynamic simulations insight into the corrosion inhibition properties of 2-(6-methylpyridin-2-yl) oxazolo [5, 4-f][1, 10] phenanthroline on mild steel. *Res. Chem. Intermed.* 39, 1927–1948.
- Olasunkanmi, L.O., Obot, I.B., Ebenso, E.E., 2016. Adsorption and corrosion inhibition properties of N-[n-[1-R-5-(quinoxalin-6-yl)-4, 5-dihydropyrazol-3-yl] phenyl] methanesulfonamides on mild steel in 1 M HCl: experimental and theoretical studies. *RSC Adv.* 6, 86782–86797.
- Ongun Yüce, A., Dođru Mert, B., Kardaş, G., Yazıcı, B., 2014. Electrochemical and quantum chemical studies of 2-amino-4-methyl-thiazole as corrosion inhibitor for mild steel in HCl solution. *Corros. Sci.* 83, 310–316. <https://doi.org/10.1016/j.corsci.2014.02.029>.
- Outirite, M., Lagrenée, M., Lebrini, M., Traisnel, M., Jama, C., Vezin, H., Bentiss, F., 2010. ac impedance, X-ray photoelectron spectroscopy and density functional theory studies of 3, 5-bis (n-pyridyl)-1, 2, 4-oxadiazoles as efficient corrosion inhibitors for carbon steel surface in hydrochloric acid solution. *Electrochim. Acta* 55, 1670–1681.
- Pearson, R.G., 1988. Absolute electronegativity and hardness: application to inorganic chemistry. *Inorg. Chem.* 27, 734–740.
- Pech-Canul, M., Bartolo-Perez, P., 2004. Inhibition effects of N-phosphono-methyl-glycine/Zn²⁺ mixtures on corrosion of steel in neutral chloride solutions. *Surf. Coat. Technol.* 184, 133–140.
- Rahmani, R., Boukabcha, N., Chouaih, A., Hamzaoui, F., Goumri-Said, S., 2018. On the molecular structure, vibrational spectra, HOMO-LUMO, molecular electrostatic potential, UV-Vis, first order hyperpolarizability, and thermodynamic investigations of 3-(4-chlorophenyl)-1-(1-lyridine-3-yl) prop-2-en-1-one by quantum chemistry calculations. *J. Mol. Struct.* 1155, 484–495. <https://doi.org/10.1016/j.molstruc.2017.11.033>.
- Ramalingam, S., David Suresh Babu, P., Periandy, S., Fereyduni, E., 2011. Vibrational investigation, molecular orbital studies and molecular electrostatic potential map analysis on 3-chlorobenzoic acid using hybrid computational calculations. *Spectrochim. Acta. A. Mol. Biomol. Spectrosc.* 84, 210–220. <https://doi.org/10.1016/j.saa.2011.09.030>.
- Ricke, J., 2018. Chapter 4 - Simulation methods: free energy calculations, Monte Carlo, molecular dynamics, and multiscale simulations. In: Ball, V. (Ed.), *Interface Science and Technology, Self-Assembly Processes at Interfaces*. Elsevier, pp. 243–250. <https://doi.org/10.1016/B978-0-12-801970-2.00004-5>.
- Rollas, S., Küçükgüzel, S.G., 2007. Biological activities of hydrazone derivatives. *Molecules* 12, 1910–1939.
- Saha, S.K., Dutta, A., Ghosh, P., Sukul, D., Banerjee, P., 2016. Novel Schiff-base molecules as efficient corrosion inhibitors for mild steel surface in 1 M HCl medium: experimental and theoretical approach. *Phys. Chem. Chem. Phys.* 18, 17898–17911.
- Salarvand, Z., Amiras, M., Talebian, M., Raeissi, K., Meghdadi, S., 2017. Enhanced corrosion resistance of mild steel in 1 M HCl solution by trace amount of 2-phenyl-benzothiazole derivatives: experimental, quantum chemical calculations and molecular dynamics (MD) simulation studies. *Corros. Sci.* 114, 133–145. <https://doi.org/10.1016/j.corsci.2016.11.002>.
- Salehi, E., Naderi, R., Ramezanzadeh, B., 2017. Synthesis and characterization of an effective organic/inorganic hybrid green corrosion inhibitive complex based on zinc acetate/Urtica Dioica. *Appl. Surf. Sci.* 396, 1499–1514.
- Sanaei, Z., Shahrabi, T., Ramezanzadeh, B., 2017. Synthesis and characterization of an effective green corrosion inhibitive hybrid pigment based on zinc acetate-Cichorium intybus L leaves extract (ZnA-CIL. L): Electrochemical investigations on the synergistic corrosion inhibition of mild steel in aqueous chloride solutions. *Dyes Pigments* 139, 218–232.
- Sastri, V., Perumareddi, J., 1997. Molecular orbital theoretical studies of some organic corrosion inhibitors. *Corrosion* 53, 617–622.
- Scully, J., Baboian, R., 1995. Standard practice for laboratory immersion corrosion testing of metals. ASTM Phila. PA, 110.
- Seah, M.P., Briggs, D., Seah, M., 1983. *Practical Surface Analysis: By Auger and X-ray Photoelectron Spectroscopy*. Wiley, New York.
- Singh, A., Ansari, K.R., Haque, J., Dohare, P., Lgaz, H., Salghi, R., Quraishi, M.A., 2018. Effect of electron donating functional groups on corrosion inhibition of mild steel in hydrochloric acid: experimental and quantum chemical study. *J. Taiwan Inst. Chem. Eng.* 82, 233–251. <https://doi.org/10.1016/j.jtice.2017.09.021>.
- Singh, P., Ebenso, E.E., Olasunkanmi, L.O., Obot, I.B., Quraishi, M. A., 2016. Electrochemical, theoretical, and surface morphological studies of corrosion inhibition effect of green naphthyridine derivatives on mild steel in hydrochloric acid. *J. Phys. Chem. C* 120, 3408–3419. <https://doi.org/10.1021/acs.jpcc.5b11901>.
- Solmaz, R., Kardaş, G., Çulha, M., Yazıcı, B., Erbil, M., 2008. Investigation of adsorption and inhibitive effect of 2-mercaptothiazoline on corrosion of mild steel in hydrochloric acid media. *Electrochim. Acta* 53, 5941–5952. <https://doi.org/10.1016/j.electacta.2008.03.055>.
- Sun, H., 1998. COMPASS: an ab initio force-field optimized for condensed-phase applications overview with details on alkane and benzene compounds. *J. Phys. Chem. B* 102, 7338–7364.
- Tang, L., Li, X., Li, L., Mu, G., Liu, G., 2006. The effect of 1-(2-pyridylazo)-2-naphthol on the corrosion of cold rolled steel in acid media: Part 2: inhibitive action in 0.5M sulfuric acid. *Mater. Chem. Phys.* 97, 301–307. <https://doi.org/10.1016/j.matchemphys.2005.08.014>.
- Tang, Y., Zhang, F., Hu, S., Cao, Z., Wu, Z., Jing, W., 2013. Novel benzimidazole derivatives as corrosion inhibitors of mild steel in the acidic media. Part I: gravimetric, electrochemical, SEM and XPS studies. *Corros. Sci.* 74, 271–282.
- Tkacz, J., Minda, J., Fintová, S., Wasserbauer, J., 2016. Comparison of electrochemical methods for the evaluation of cast AZ91 magnesium alloy. *Materials* 9, 925.
- Umoren, S.A., Eduok, U.M., Solomon, M.M., Udoh, A.P., 2016. Corrosion inhibition by leaves and stem extracts of *Sida acuta* for mild steel in 1M H₂SO₄ solutions investigated by chemical and spectroscopic techniques. *Arab. J. Chem.* 9, S209–S224. <https://doi.org/10.1016/j.arabjc.2011.03.008>.
- Verma, C., Ebenso, E.E., Bahadur, I., Quraishi, M., 2018. An overview on plant extracts as environmental sustainable and green corrosion inhibitors for metals and alloys in aggressive corrosive media. *J. Mol. Liq.*
- Weder, N., Alberto, R., Koitz, R., 2016. Thiourea derivatives as potent inhibitors of aluminum corrosion: atomic-level insight into adsorption and inhibition mechanisms. *J. Phys. Chem. C* 120, 1770–1777. <https://doi.org/10.1021/acs.jpcc.5b11750>.

- Weng, L., Poleunis, C., Bertrand, P., Carlier, V., Sclavons, M., Franquinet, P., Legras, R., 1995. Sizing removal and functionalization of the carbon fiber surface studied by combined TOF SIMS and XPS. *J. Adhes. Sci. Technol.* 9, 859–871.
- Wong, M.W., Frisch, M.J., Wiberg, K.B., 1991. Solvent effects. 1. The mediation of electrostatic effects by solvents. *J. Am. Chem. Soc.* 113, 4776–4782. <https://doi.org/10.1021/ja00013a010>.
- Wypych, G., 2017. 10 - MOLECULAR DYNAMICS SIMULATION. In: *Self-Healing Materials*. ChemTec Publishing, pp. 93–95. <https://doi.org/10.1016/B978-1-927885-23-9.50012-2>.
- Xie, S.-W., Liu, Z., Han, G.-C., Li, W., Liu, J., Chen, Z., 2015. Molecular dynamics simulation of inhibition mechanism of 3,5-dibromo salicylaldehyde Schiff's base. *Comput. Theor. Chem.* 1063, 50–62. <https://doi.org/10.1016/j.comptc.2015.04.003>.
- Yilmaz, N., Fitoz, A., Ergun, Y., Emregül, K.C., 2016. A combined electrochemical and theoretical study into the effect of 2-((thiazole-2-ylimino)methyl)phenol as a corrosion inhibitor for mild steel in a highly acidic environment. *Corros. Sci.* 111, 110–120. <https://doi.org/10.1016/j.corsci.2016.05.002>.
- Yıldız, R., Doğan, T., Dehri, İ., 2014. Evaluation of corrosion inhibition of mild steel in 0.1M HCl by 4-amino-3-hydroxynaphthalene-1-sulphonic acid. *Corros. Sci.* 85, 215–221. <https://doi.org/10.1016/j.corsci.2014.04.017>.
- Zarrouk, A., Hammouti, B., Lakhlifi, T., Traisnel, M., Vezin, H., Bentiss, F., 2015. New 1H-pyrrole-2, 5-dione derivatives as efficient organic inhibitors of carbon steel corrosion in hydrochloric acid medium: electrochemical, XPS and DFT studies. *Corros. Sci.* 90, 572–584.
- Zhou, J., Chen, S., Zhang, L., Feng, Y., Zhai, H., 2008. Studies of protection of self-assembled films by 2-mercapto-5-methyl-1, 3, 4-thiadiazole on iron surface in 0.1 M H₂SO₄ solutions. *J. Electroanal. Chem.* 612, 257–268.